TECHNICAL MEMORANDUM

ANL-CT-82-7

Distribution Category:
LMFBR—Components: Base Technology (UC-79k)

ANL-CT--82-7

DE82 014905

ARGONNE NATIONAL LABORATORY
9700 South Cass Avenue
Argonne, Illinois 60439

DESIGN GUIDE FOR SINGLE CIRCULAR CYLINDER IN TURBULENT CROSSFLOW

by

T. M. Mulcahy

Components Technology Division

March 1982

TABLE OF CONTENTS

LIST OF FIGURES

LIST OF TABLES

c_i	Reduced modal damping for ith mode, see (2)
C_D	Steady drag force coefficient
C_{DU}	Measured C_D uncorrected for test section blockage
C'_D	Fluctuating drag force coefficient (RMS)
C'_{DC}	Calculated C'_D, see (15)
C_L	Lift force coefficient (RMS), see (1)
C_{LR}	Random component of C_L, see (18)
C_{LV}	Periodic component of C_L, see (18)
C( )	Viscous damping operator per unit length
D	Cylinder diameter
f	Frequency, cycles/sec (Hz)
Δf	Half-power bandwidth of lift force spectra
$\bar{f}$	fD/V, reduced frequency
$\bar{f}_o, \bar{f}_v$	$\bar{f}$ for f_o and f_v, respectively
f_o, f_i	Lowest structural mode natural frequency, ith mode frequency
f_V	Vortex shedding frequency
F_V, F_B, F_R	Reduced fluid loading forces, see (22-24)
h	Water depth
i,j	Subscripts denoting structural vibration modes; i,j = 0, 1, 2, ...
$\hat{i}$	Imaginary constant, $\sqrt{-1}$
k_i	Modal stiffness, $m_i\omega_i^2$
K	Reduced stiffness, see (21). Constant employed in [28]
ℓ_c	Correlation length of fluid forces, see (10)
L	Beam length
L_c	Constant value of ℓ_c
L_e	Portion of beam length subject to crossflow
L_u	Flow direction turbulence integral scale length
L( )	Stiffness operator per unit length
m	Beam mass/length
m_i	Modal beam mass/length for ith mode, see (9)
$m_A(x)$	Added fluid mass, see (4)
$m_c(x)$	Contained fluid mass, see (4)
$m_s(x)$	Structural mass, see (4)
m_t	$m_A + m_c + m_A$
M_i	Effective modal mass/length, see (3)
N_R	VD/ν, Reynolds number
p	Fluid force component/unit beam length
p_i	Modal force per unit length
P_i	Fourier transform of p_i
$\langle p_V^2 \rangle$	Mean-square lift force/beam length due to vortex shedding
q_i	Modal displacement
Q_i	Fourier transform of q_i
r_i	Free vibration response component, Appendix A
$r(x,x',f)$	Coherence function, see (
R_p	Autocorrelation of p
S	Strouhal number, $f_V D/V$
ΔS	$\Delta f D/V$
S_{ij}	Cross spectral density of ($-\infty \leq f \leq \infty$)
$S_p(x,f)$	Fluid force spectral dens
$S_p(x,x',f)$	Fluid force cross spectra
t	Time
u	Fluctuating component of
$\langle u^2 \rangle^{1/2}/V$	Flow direction turbulence
V	Mean crossflow velocity
V_M	Maximum value of V over I
V_{ri}	$V/f_i D$, reduced velocity f
V_{rs}	$1/S = V/f_V D$
w	Beam lateral displacement
W	Fourier transform of w
$\langle w^2 \rangle$	Beam mean square lateral
x,x'	Locations along beam axis
z_i	Structural amplification
$\gamma_V, \gamma_B, \gamma_R$	Amplification factors, se
Δ	Small correlation length
ζ_i	Damping factor, fraction
ν	Fluid kinematic viscosity
ξ, ξ'	Dummy variables
ρ	Fluid mass density
ϕ_D	Fluctuating drag spectral
ϕ_L	Wide-band, lift force spe
ϕ_p	Spectral density ($0 < f <$
ϕ_{ij}	Cross spectral density of
Φ	Normalized turbulent flow
Φ_D	Normalized fluctuating dr
Φ_{DO}	Φ_D for $\bar{f} = 0$
Φ_L	Normalized wide-band, lif
Φ_{LO}	Φ_L for $0 < \bar{f} < 0.22$
Φ_o	Φ for $\bar{f} = 0$
Φ_p	Normalized force spectral
Φ_{ij}	Normalized ϕ_{ij}
ψ_i	ith mode shape function,
ω	Frequency, radians/sec
ω_i	Beam ith modal frequency,
$( )^*$	Denotes complex conjugate
$(\dot{})$	Denotes time derivative

tion, see (8)
n of p
r, $f_V D/V$

density of generalized modal forces

ectral density ($-\infty < f < \infty$)
oss spectral density ($-\infty < f < \infty$)

mponent of crossflow in mean flow direction
turbulence intensity
velocity
of V over L_e
velocity for structural frequency f_i

isplacement
orm of w
re lateral displacement
g beam axis
lification factor, see (8)

factors, see (25-27)
ion length
, fraction of critical damping, for ith mode
c viscosity
s
sity
ag spectral density ($0 < f < \infty$), see (15)
t force spectral density ($0 < f < \infty$), see (16)
ty ($0 < f < \infty$) of p(x,t)
density of generalized modal forces ($0 \leq f \leq \infty$)
bulent flow spectral density, see (11)
ctuating drag spectral density, see (13)

e-band, lift force spectral density, see (16)
< 0.22

ce spectral density, Φ_D or Φ_L

function, eigenvector, see (3)
ians/sec
frequency, radians/sec
x conjugate of complex function
erivative $\frac{d}{dt}$ ( )

ABSTRACT

A design procedure is proposed for predicting the dynamic structural response of a circular cylinder in turbulent crossflow. The procedure is based on recently obtained data for a stationary, rigid cylinder and on existing information. The procedure is not applicable to conditions where the wake vortex shedding frequency locks in to a structural natural frequency.

This report is self-contained in that all the information and structural analysis methods employed in the procedure are reviewed and developed. Also, an example is given to illustrate the use of the method for a typical reactor component. The calculated responses are found to be very small.

INTRODUCTION

The response of a circular cylinder to flow normal to its longitudinal axis, called crossflow, involves very complex physical phenomena which are the subject of current research. Because a single tube in crossflow is not an uncommon reactor geometry and strong fluid excitation mechanisms may exist, the associated response must be accounted for in fatigue or fretting and wear design. Several methods of response analysis and bodies of data describing the fluid forces are available upon which to base a design guide. The methods of structural analysis are classical, but the applicability of the force data available and the modeling of the fluid-structure interaction are controversial.

To date, most structural response analyses have been based on information obtained for cylinders with very smooth surfaces subject to the two-dimensional, uniform, very low turbulence, crossflow producible in wind and water tunnels. These conditions shall be referred to as "ideal crossflow." For ideal crossflow, for which the fluid forces due to periodic vortex shedding can be large and highly correlated along the cylinder length, large responses are predictable, especially when the frequency of the vortex shedding and the natural frequency of the structure coincide or are multiples of each other. The vortex shedding is amplified by the structural motion, and vice versa, with bounded steady state motion resulting. The amplitude of the motion can be quite large depending on the structural and fluid frequencies, mass, and damping. The worst case occurs when the vortex shedding frequency "locks in" [1] to a structural mode frequency. However, not uncommonly, reactor scale model response measurements with potentially detrimental, but other than ideal, crossflow conditions fail to show anything but relatively low level random motion [2] with no hint of periodic vortex shedding induced excitation. In short, current design methods based on ideal crossflow information appear conservative.

As more and more is learned about the crossflow excitation mechanisms, the design methods can be made more specific, and, as a result, less conservative and more accurate. Recently obtained experimental data [3] for an isolated, stationary and rigid, smooth surfaced cylinder indicate that the fluid forces can be greatly altered when the free stream turbulence in the crossflow is significant. The magnitude of the fluid forces may be greatly reduced and thus be less effective in producing structural

response, at least when the vortex shedding and structural motion do not interact.

Based on this new data, a design procedure is proposed here which attempts to account for the effects of turbulence in the flow. Its full range of validity is yet to be determined, and the author requests feedback where comparisons with measured response or prediction of other design methods are performed. In particular, in this design procedure, fluid-structure interaction and the lock-in phenomenon are precluded by limiting application to structures which are relatively heavily damped and for which the nominal vortex shedding frequency is removed from the structural natural frequency. There is some evidence [40] that lock-in does not occur for relatively turbulent flows, but much more research is required before its existence can be precluded. Until then, other design methods [1,14, 16,19,21] which account for lock-in should be employed when the conditions for lock-in cannot be precluded. Of course, this design procedure can also be applied for lock-in conditions and is recommended where experimental measurement of prototypic response is planned. Comparisons with both predictions would be important in determining the existence of the lock-in phenomenon in practical reactor system flows.

This design procedure provides a considerable amount of background information, to provide completeness, but the Design Procedure section stands alone and can be employed separately by those who know too much or too little.

DESIGN INFORMATION

The pertinent literature is reviewed and information presented which will enable the performance of a linear elastic dynamic structural analysis of a circular cylindrical component subject to turbulent crossflow. In particular, characterizations of the fluid forces, a structural analysis method, and criteria to avoid nonlinear fluid-structure interaction excitation and lock-in are specified. Because the fluid forces created by turbulent flow are primarily random in nature, a probabilistic formulation is necessary.

1. Fluid Forces

In ideal crossflow, the strongest vibration excitation mechanism is associated with the time varying (periodic to random) lift force component created by vortices shed in the wake of the cylinder. The fluctuating lift force acts normal to the cylinder axis and mean flow direction: the lift direction. A usually larger steady drag force and a relatively smaller fluctuating drag force component are created normal to the cylinder axis and parallel to the mean flow direction: the drag direction. For a rigid, stationary cylinder the primary independent parameter is the Reynolds number N_R, based on the mean velocity V and the cylinder diameter D.

In turbulent crossflow, the mean square distribution of the lift force in the frequency domain, called the lift force spectral density, appears to consist of a component in a narrow band of frequencies, due to organized vortex shedding, superimposed on a component which occurs over a wide band of frequencies primarily below the vortex shedding frequency, due to flow turbulence in the free stream and turbulence in the wake. The relative size of the two components depends upon N_R and the turbulence of the free stream. As a minimum, the flow turbulence should be characterized in terms of the flow direction turbulence intensity $\langle u^2 \rangle^{1/2}/V$ and its integral scale length L_u.

The turbulence intensity $\langle u^2 \rangle^{1/2}/V$ is a measure of the relative size of the root mean square value of the fluctuating part of the flow direction velocity component u relative to the mean value V. Typically wind and water tunnels have turbulence intensities of less than 1%, while pipe and wall-turbulent shear flows have intensities from 4 to 8% depending upon distance from the wall and direction with respect to the mean flow direction. Mixing regions in reactor plenums and heat exchangers may have

greater than 15% intensity especially where separated shear layers occur downstream of grids, screens, tube arrays, and sudden changes in flow channel dimensions.

The integral scale length L_u is a measure of the average size turbulent eddy creating the velocity fluctuations in the flow direction. Its magnitude is governed by the size of the geometry creating the disturbance: the bar size and spacing for screens and grids, the radius for pipe flow, and the boundary layer thicknesses for shear flows along walls. For homogeneous, isotropic turbulence well defined relations exist between the size and decay of the directional components of the intensities, integral scales and other point measures of the character of the turbulence. In practical flows, such ideal conditions can only be approached, and the character of the turbulence must be measured [24]. Typically for reactor components mean velocity information is available, turbulence intensity information may be available if a detailed study of thermal mixing has been made, and the integral scale sizes must be estimated.

Besides the flow turbulence, other factors such as surface roughness, flow gradients, and yaw of the cylinder with respect to the mean flow direction will affect the fluid forces [6,25]. Yaw effects can be conservatively accounted for by using the component of velocity normal to the cylinder as the mean velocity. Where a flow gradient occurs, replacing it with one or more uniform flows having the maximum velocity in the flow gradient usually is a conservative approximation. Neglecting surface roughness often, but not always, produces a conservative design. Each of these items is the subject of current research which should be consulted for further information. They will not be considered further. The purpose of this guide is to further quantify the effects of turbulent flow.

a. Ideal crossflow

Much about the character of the narrow band component of the fluid forces in turbulent flow can be ascertained from the large amount of data obtained for a stationary cylinder subject to ideal crossflow.

For $10^3 < N_R < 3 \times 10^5$, subcritical Reynolds numbers, the narrow band component is believed due to the two-dimensional tendency of the separated boundary layer to roll into distinct vortex sheets along the axis of the cylinder and shed alternatively from the top and bottom of the cylinder at frequencies centered around a Strouhal number S of 0.19 based on

cylinder diameter D and mean, free stream velocity V. See Fig. 1(a) for mean values of S for different N_R based on a recent compilation of data [5]. For ideal crossflow, vortex shedding correlation lengths of three to six diameters have been measured for subcritical Reynolds numbers and the amplitude of the associated lift force is nearly periodic [6]. When the mean-square magnitude of the lift force per unit length is defined according to

$$\langle p_V^2 \rangle = \left(\frac{1}{2} \rho V^2 D\right)^2 C_L^2 , \qquad (1)$$

the lift coefficient C_L varies with N_R as shown in Fig. 2(a).

In the drag or flow direction both a mean and fluctuating force exist and coefficients C_D and C_D', respectively, can be defined similar to the lift coefficient in (1). Typically, C_D' has a value of one-tenth and C_D is of the same order as C_L; see Figs. 3(b) and 4. As could be expected, the fluctuating force frequency energy content is centered at twice the vortex shedding frequency. However, the energy apparently has been observed to occur over a broader frequency band than occurs for the associated lift. Presumably [25] the fluctuating drag force is more sensitive to 3-D flow effects than the fluctuating lift.

For larger N_R ($> 3 \times 10^5$), the attached boundary layer undergoes a turbulence transition extending to $N_R = 3\text{-}4 \times 10^6$, the critical region. The transition process destroys the two-dimensionality of the vortices and the RMS lift and drag coefficients, Figs. 2(a) and 3(a), are reduced from the values in the subcritical range, with a frequency content existing over gradually peaked wide bands. The S versus N_R curve of Fig. 1(a) is shown dashed in this region to indicate the trend of the very sporadic data in this region. Periodicity is not believed to exist, but various anomalies have resulted in reports of periodicity [5]. Correlation lengths on the order of one cylinder diameter have been reported but the data is sparse [6-8].

The data for $N_R > 4 \times 10^6$, the transcritical region, is even sparser than for the critical region. However, a return to a narrow band random frequency content and finally to almost periodic distributions by $N_R = 6 \times 10^6$ have been reported [6-12] for the lift force, but no indication of periodicity in the fluctuating drag has been reported [24]. Up to 6 x

10^6, the only available data [7] indicates a correlation length of only one cylinder diameter. Simulated transcritical flows for $N_R > 10^6$ have produced correlation lengths on the order of nine diameters [9] and larger lift coefficients, but to simulate the transcritical N_R the model surfaces had to be significantly roughened producing a boundary layer flow which may be unique to roughened surfaces [15].

b. Turbulent flow

The effect of turbulence in the flow on fluid forces is threefold, with all effects resulting in spectral densities which are more random than periodic. First, the Reynolds number at which the attached boundary layer undergoes transition from laminar to turbulent flow is reduced [3,25,26]. This can be observed from the relatively sharp declines in C_L and C_D in Figs. 2(a) and 4, as well as in the increase in ΔS in Fig. 1(b). Thus, the critical region appears to occur over a larger Reynolds number range, and the associated wake forces are random at N_R where they were periodic in ideal crossflow: the more turbulent the flow, the smaller the subcritical range of Reynolds numbers. The existence of a transcritical region in turbulent crossflow cannot be determined until more tests in turbulent flow at higher N_R have been performed.

No hint of a return to narrow band or periodic fluid forces typical of the transcritical range in ideal crossflow has been observed in turbulent flows with $2 < \langle u^2 \rangle^{1/2}/V < 15\%$ and $N_R < 5 \times 10^5$ [3,26], but a return in the pressure field has been reported [25]. One would expect a transcritical region to exist for only slightly turbulent flows, meaning the possibility cannot be ruled out. Thus a conservative estimate of the beginning of the transcritical region in turbulent flow, at least for $\langle u^2 \rangle^{1/2}/V < 0.15$, would be $N_R = 8 \times 10^5$. This estimate is based on the elimination of the subcritical range by the turbulence and the existence of the same size critical range as occurs for ideal crossflow.

The second effect of turbulence in the flow is the degradation of the two-dimensional vortex shedding process for subcritical Reynolds numbers, as measured by the broadening and reduction in amplitude of the vortex shedding peaks in the lift force spectral densities [3,25-27]. For large turbulence intensities this effect is difficult to distinguish from the effect of an earlier transition to the critical region, as discussed previously. But, for whatever reason, the axial correlation of the surface

pressures and forces are the same size or smaller than in ideal crossflow. Based on this information, together with the knowledge that many cylinder end effects lead to the almost total breakdown of two-dimensional flow to three-dimensional flow [3,5-14,25], axial correlation lengths in practical flow situations can be expected to be less than 3D for subcritical Reynolds numbers and D for other Reynolds numbers.

The third effect is the pressure fluctuations created, at least on the upstream side of the cylinder surface [27], by the impinging turbulence in the flow. The associated random excitation forces are difficult to separate from those created by the wake. However, the relative magnitude of the drag coefficient with respect to the lift coefficient is larger in turbulent flow than in ideal crossflow. See Fig. 3(b). Periodicity may still exist in the drag direction, but for the most part it is submerged in the wide band random forces which the turbulence in the flow somehow creates. Utilizing turbulent flow drag force data is more conservative than using ideal crossflow data.

2. Fluid-Structure Interaction

Interaction of the structure with the wake flow resulting in amplified motion and lock-in has been observed for several parameter ranges. Lock-in definitely can occur for subcritical Reynolds number in nonturbulent flow [6]. Its existence in the critical range is debatable and expected in the transcritical [17]. Practical occurrences have been documented in all ranges [18], so the possibility must be assessed for all Reynolds numbers in turbulent flow. In ideal crossflow the phenomenon only occurs for specific excitation frequency ranges and structural mass and damping parameters.

Lock-in in the lift direction, normal to the flow, may occur at reduced velocities $V_{ri} = V/f_i D$ within ±25% of the vortex shedding reduced velocity $V_{rs} = 1/S$ [6], at least for subcritical N_R ($< 2 \times 10^5$). Since S is ~0.2, fluid interaction with lift direction structural motion can be avoided if $V_{ro} < 3.75$ can be achieved by design. If coincidence of the vortex shedding and lowest structural natural frequency cannot be avoided as proposed above, then the design must be rationalized utilizing one of the several currently proposed analysis methods [1,14,16,19, 21] which account for the lift direction lock-in or by scale model testing [22]. Lift direction lock-in is a strong excitation mechanism and can occur for a

wide range of structural densities, fluid densities, and structural damping.

Lock-in, or at least fluid-solid interaction which may significantly amplify drag or flow direction structural motion, has been observed to begin at one-quarter V_{rs} [16]. Lock-in at one-half V_{rs}, corresponding to twice the shedding frequency, is not unexpected, because the vortex shedding process is asymmetric: at least, vortices are shed alternatively from each side of a stationary cylinder. However, the basis for fluid-structure interaction at three and four times the shedding frequency is not obvious and is the subject of current research [16,19,20]. Fluid interaction with drag direction structural motion can be avoided if $V_{ro} < 1$ can be achieved by design. This condition also avoids possible structural excitation by the weaker higher frequency harmonics of the shedding process [1] for which little information is available.

Drag direction, compared to lift direction, fluid-structure interaction is a relatively weak excitation mechanism, and usually only occurs for lightly damped structures in dense fluids (liquids). For cantilevered cylinders of length L subject to various levels $h \leq L$ of flow above the base, a geometry representing ocean piles, fluid structure interaction apparently is suppressed [16] if the reduced structural damping c_i satisfies

$$c_i = \frac{4\pi\zeta_i M_i}{\rho D^2} > 1.2 \ , \tag{2}$$

where ζ_i is the fraction of critical damping in the ith vibration mode and M_i is the effective modal mass per unit length given by

$$M_i = \frac{\int_o^L m_t(\xi)\psi_i^2(\xi)d\xi}{\int_{L_e} \psi_i^2(\xi)d\xi} \ , \tag{3}$$

with ψ_i the ith mode shape function, to be discussed more in the next section, and $m_t(\xi)$ the beam mass per unit length. The range L_e in the denominator implies integration should occur only over the region of the cylinder length subject to crossflow, which, for an ocean pile, is the water depth h. Also note that m_t is composed according to

$$m_t(x) = m_s(x) + m_c(x) + m_A(x) \ , \tag{4}$$

where m_s is the structural mass, m_c the contained fluid mass, and m_A the added fluid mass. For an isolated cylinder, m_A is the displaced fluid mass. If sections of the cylinder are confined then the possibility of increased added mass and fluid damping must be taken into account [23,28].

Because a cantilevered cylinder loaded at its free end represents a geometry most susceptible to flow excitation, except possibly for a rigid cylinder with each end spring mounted, satisfaction of (2) for a more general structure would likely avoid drag direction lock-in. In more general use of (2), L_e would represent the region along the cylinder where significant vortex shedding is occurring.

In the design method proposed here, satisfaction of (2) and

$$V_{ro} < 3.33 \tag{5}$$

is required. This limit is proposed to exclude lock-in at subcritical N_R as well as at larger N_R where $S > 0.2$ can occur; see Fig. 1(a). If neither condition can be satisfied, then the design must be rationalized utilizing existing analysis methods or scale model testing [22]. Most likely scale model testing will be required because of lack of analysis information.

3. Response Equations

The response equation can be greatly simplified because of the design restriction imposed to avoid fluid-structure interaction. If, in addition, the beam response is assumed to be linear and separable into normal modes, see Appendix A, the mean square value of the lateral displacement is

$$\langle w^2 \rangle = (\psi_o^2/k_o^2) \int_o^\infty \phi_{oo}/|z_o|^2 df \ . \tag{6}$$

The expression for $\langle w^2(x) \rangle$ only contains contributions from the lowest frequency vibration mode $\psi_o(x)$, because the main energy of excitation is restricted by (2) and (5) to occur substantially below the fundamental mode frequency f_o. In addition, beam frequencies normally are widely separated. The mode shape ψ_o and the fundamental frequency f_o are either measured or calculated via free vibration analysis (see Appendix A).

The fundamental modal stiffness in (6) is

$$k_o = m_o(2\pi f_o)^2 \tag{7}$$

where the fundamental modal mass per unit length is determined by

$$m_o = \int_o^L m_t \psi_o^2 d\xi \; / \; \int_o^L \psi_o^2 d\xi \tag{8}$$

in terms of the total mass per unit length $m_t(x)$ which is measured or estimated and includes contained liquid and added mass as indicated in (4). The magnitude of the amplification factor for the fundamental mode is

$$|z_o|^2 = [1 - (f/f_o)^2]^2 + [2\zeta_o f/f_o]^2 \tag{9}$$

where ζ_o is the measured or estimated fraction of critical viscous damping in the fundamental mode for nonflowing fluid.

The fundamental mode's generalized force spectral density can be approximated by

$$\phi_{oo} = [\int_o^L \psi_o^2 d\xi]^{-2} \int_o^L \phi_p \ell_c \psi_o^2 d\xi \tag{10}$$

because the correlation length $\ell_c(x,f)$ of vortex shedding in turbulent flow can be expected to be substantially less than the beam length. Based on the data described in the previous section $\ell_c < 3D$. Without this simplification, $\phi_{oo}(f)$ would depend upon cross correlations and cross spectral densities of $p(x,t)$ instead of the easier to obtain single point spectral density $\phi_p(x,f)$. See Appendix A. Available results for the single-sided ϕ_p, $0 < f < \infty$, will be presented in the next section.

4. Fluid Force Coefficients and Spectral Densities

Fluctuating lift and drag force spectral densities have been measured [3] for a wide range of flow direction turbulence intensities (1.5 to 15%) and integral scale lengths (0.5 to 2 times the cylinder diameter D). The functional form of these single sided ($0 \leq f \leq \infty$) force spectra was approximated using the normalized one-dimensional velocity fluctuation spectrum for homogeneous, isotropic turbulent flow [24]

$$\Phi(\bar{f}) = \Phi_o(1 + 4\pi^2\bar{f}^2)^{-1} \tag{11}$$

which is graphed in Fig. 5 for $\Phi_o = 4.5$ as a function of the reduced frequency

$$\bar{f} = fD/V, \tag{12}$$

where V is the mean crossflow velocity. The velocity fluctuation spectra also were measured [3] and found to be well approximated by (11) when, instead of D in (12), the measured integral length scale in the flow direction, L_u, was employed.

a. Fluctuating drag

The functional form for the normalized fluctuating drag spectra was chosen to be

$$\Phi_D(\bar{f}) = \Phi_{DO}(1 + 4\pi^2\bar{f}^2)^{-1} \tag{13}$$

where Φ_D is a normalization of ϕ_D, the single-sided spectral density of the fluctuating fluid drag force per unit length. Specifically,

$$\Phi_D = \phi_D(V/D)(1/2\ \rho V^2 D)^{-2}. \tag{14}$$

A Φ_{DO} was chosen for each turbulence condition such that Φ_D formed an upper bound on the wide band part of the spectra for all values of Reynolds number N_R. Table 1 associates the Φ_{DO} chosen with the turbulence condition and the RMS fluctuating drag force coefficient C'_{DC} calculated by integrating (13) from zero to infinity

$$(C'_{DC})^2 = 0.225\ \Phi_{DO}\ . \tag{15}$$

The degree to which (13) approximates the measured spectra is well represented by the differences between the calculated C'_{DC}, given in Table 1, and the measured C'_D shown in Fig. 3(b). Except for the lowest N_R and grid 2 data, (13) represented the spectra well: the spectra are nearly the same for the same turbulence condition and different N_R. Some narrow band content in the measured drag fluctuation data was present at multiples of the vortex shedding Strouhal number, but it was typically submerged in the wide band excitation forces except at the lowest Reynolds numbers. By adding to the wide band excitation forces a deterministic force at $\bar{f} = 0.4$ with a coefficient of $(C'_D - C'_{DC})$, when $C'_D > C'_{DC}$, an upper bound on the fluctuating fluid drag force can be generated.

b. Fluctuating lift

The spectra of the fluctuating lift force per unit beam length could not be as simply approximated as could the fluctuating drag spectra,

because a relatively large component of force in a narrow frequency band was superimposed upon components of forces extending over a wide frequency band. The narrow band was centered around the vortex shedding frequency corresponding to the Strouhal number S, which averaged 0.19 for the N_R tested. As the turbulence intensity increased, the bandwidth of the narrow band component broadened until only a band limited component existed. Thus the measured Strouhal numbers represent peak frequencies of the lift spectra, and they are given in Table 2 and compared in Fig. 1(a) to the data obtained in ideal crossflow. A measure of the randomness of the narrow band component can be gleaned from Fig. 1(b) and Table 2 where the half-power bandwidth, in terms of the Strouhal number ΔS, is shown as a function of turbulence character and Reynolds number, as well as compared to ideal crossflow ΔS. For ideal crossflow, $\Delta S \sim 0$ for $N_R < 2 \times 10^5$. Also, ΔS is difficult to define in the critical region, $2 \times 10^5 < N_R < 3 \times 10^6$, where no reproducible peaks exist in the lift spectra.

The wide band component of the lift force spectra for $\bar{f} < S$ appeared to be representable by Φ, while for $\bar{f} > S$ it appeared to be representable by Φ^2. See Fig. 5 for Φ, Φ^2, and a linear approximation Φ_L which differed from the measured spectra mainly where the narrow band component existed. Thus the wide band component of the normalized lift spectra was represented by

$$\begin{aligned} \Phi_L &= \Phi_{LO} && \bar{f} < 0.22 \\ &= (2.34 \times 10^{-3})\Phi_{LO}\bar{f}^{-4} && \bar{f} > 0.22 \end{aligned} \tag{16}$$

where Φ_L is related to the single-sided spectral density of the fluctuating lift force per unit length ϕ_L by

$$\Phi_L = \phi_L(V/D)(1/2\ \rho V^2 D)^{-1/2}. \tag{17}$$

The narrow band component was represented by a deterministic force at $\bar{f} = 1/S = 0.2$ with a lift coefficient

$$C_{LV} = C_L - C_{LR} \tag{18}$$

where C_L is the measured lift coefficient and C_{LR} is a calculated value associated with the wide band component: the area under the curve (16) from

$\bar{f} = 0$ to ∞ for a Φ_{LO} selected to best fit (visually) the experimental data

$$C_{LR}^2 = 0.293\ \Phi_{LO}. \tag{19}$$

The lift coefficients are displayed in Figs. 2 and 3(a) as well as listed in Table 2 for each Φ_{LO}.

c. Mean drag

The measured mean drag coefficients C_D are plotted in Fig. 4, and listed in Table 2, along with bounding curves for the existing nonturbulent flow data. Note that the C_D are corrected for test section blockage [4], and the uncorrected values C_{DU} are listed in Table 2. The fluctuating lift and drag coefficients were not corrected for blockage because no agreed upon method exists. The significant reduction in drag due to flow turbulence is most apparent in Fig. 4 and thought to be due to transition of the attached boundary layer to a state of turbulence at a lower Reynolds number than occurs for nonturbulent flows.

5. Design Equations

If the velocity and correlation length distributions, $V(x)$ and $\ell_c(x,f)$, are known in detail, then expressions for the fluctuating lift and drag forces could be obtained from (13), (16), and (19) and substituted into (10) and (6) to obtain the mean square response. However, such detailed information is rarely known with sufficient accuracy to warrant this rigorous approach.

Typical of industrial applications, a maximum velocity is available, $V = V_M$, along with a length L_e over which significant fluid loading is expected to occur, and the designer must estimate the correlation length $0 < \ell_c < 6D$. Assuming uniform flow velocity and constant correlation length L_c, the mean square fundamental mode response is (see Appendix A)

$$\frac{\langle w^2 \rangle}{\psi_o^2(x) D^2} \approx \frac{1}{K^2} \left(\gamma_V F_V^2 + \gamma_B F_B^2 + \gamma_R F_R^2 \right), \tag{20}$$

where a reduced stiffness K has been defined

$$K^2 = (4\pi \bar{f}_o^2 c_o)^2 / (2\zeta_o)^2 \tag{21}$$

which is independent of damping ζ_o. Reduced forces have been defined

$$F_V^2 = C_{LV}^2 \tag{22}$$

$$F_B^2 = C_{LR}^2 \tag{23}$$

$$F_R^2 = \bar{f}_o \Phi_p(\bar{f}_o) \tag{24}$$

for periodic vortex shedding, turbulent buffeting, and turbulent excitation of resonant response, respectively. The remaining terms are combined fluid and structure multipliers for each type of force

$$\gamma_V = \left(L_c / \int_{L_e} \psi_o^2 d\xi\right) \left[(1 - \bar{f}_V^2/\bar{f}_o^2)^2 + (2\zeta_o \bar{f}_V/\bar{f}_o)^2\right]^{-1} \tag{25}$$

$$\gamma_B = L_c / \int_{L_e} \psi_o^2 d\xi \tag{26}$$

$$\gamma_R = \left(L_c / \int_{L_e} \psi_o^2 d\xi\right)\left(\frac{\pi}{4}\, \zeta_o^{-1}\right) . \tag{27}$$

A different correlation length L_c may be employed for each type of reduced force when available.

DESIGN PROCEDURE

Based on the preceding information, a procedure to estimate the mean square displacement of an isolated, smooth surfaced, circular cylinder in turbulent crossflow has been developed. The fluid-structure interaction, where the vortex shedding frequency locks-in with a structural natural frequency, is avoided by component design. The main purpose of this procedure is to account for the effects of turbulence in the flow stream. The effects of a roughened cylindrical surface [9,15] or adjacent structures [14,26], which can be significant, are not accounted for, but the same method can be applied when fluid force data becomes available.

1. Structural Characterization

Use of the procedure presumes the following structural information is available: (a) the measured or calculated fundamental (lowest) structural frequency f_o and mode shape $\psi_o(x)$ of the circular cylindrical structure in a still fluid, (b) the fraction of critical damping ζ_o which occurs during fundamental mode free vibration in a still fluid, and (c) the total mass of the beam per unit length $m_t(x)$ which is composed, see (4), of the structural mass plus any contained fluid mass plus any added fluid mass.

In calculating f_o and $\psi_o(x)$, the total $m_t(x)$ should be employed when the cylinder is immersed in a dense fluid (liquid): usually the contained and added fluid mass are not negligible in comparison to the structural mass especially if thin-walled tubes are part of the design. Determination of the contained fluid mass and the added fluid mass for an isolated circular cylinder, the displaced fluid mass, is simple. However, if portions of the cylinder's surface are separated from adjacent structures by less than one cylinder diameter, a confined structure, then much larger added mass may occur which can be estimated by available literature [23,28].

The total fraction of critical damping ζ_o in a still fluid is best obtained by measurement, but prototype values normally are not available during design. If damping values are available from a scale model test, then scrutiny of the data is necessary to avoid overestimation of damping values due to scale modeling distortions [22,33,34]. Clearly the goal is to just underestimate the prototype damping to produce a design which is conservative but not overly conservative. However, the procedure for determination of ζ_o is not well defined especially when test values are not available.

Without test data, estimates of ζ_o must be made based on information obtained for structures of like design. As a starting point see [22,31-32,34-35]. Similarity of the structure from which ζ_o is estimated cannot be overemphasized, because values of ζ_o can vary greatly depending upon the type of structural connections and fluid confinement. For instance, welded joints can result in very low fractions of critical damping, less than 0.005, whereas the slip joints of heat exchanger baffle supports [1] or fuel assembly grid supports [32] may produce large damping values, greater than 0.10. Adjacent bodies, closer than one-half diameter and creating a confined structure, can produce large damping values [23,28] by the same effect which makes fluid bearings possible. Often damping values obtained in air are employed, because they are smaller than submersed values and thus give conservative response estimates. In any case, the inaccuracy in obtaining damping values should be understood for it is reflected directly in response predictions. Also, it should temper the rigor employed in the application of the design procedure.

2. Hydraulics Characterization

As a minimum, the local velocity distribution producing crossflow must be known to the extent that a maximum mean flow velocity V_M and the cylinder length L_e over which significant crossflow occurs can be defined. If significant gradients exist in the flow velocity distribution along the cylinder, then the fluid loading may be broken into several regions with several maximum flow velocities. After subdivision, the procedure can be applied to each region separately, and the mean square responses obtained by superposition. However, the lengths of the regions should be no smaller than the vortex shedding correlation length L_c chosen in the procedure. Also, if the mean flow velocity does not act normal to the axis of the cylinder, then the component normal to the axis should be employed.

Since Reynolds number N_R is important in determining vortex shedding flow regimes, the fluid viscosity ν must be known. While ν is relatively easy to determine, the flow turbulence parameters, which also affect flow regimes, are not normally available and may pose the main obstacle to the use of this design procedure.

To apply the design procedure, estimates must be made of the turbulence intensity and integral scale lengths in the flow direction. However, only crude estimates are required because of the scatter in the limited

data available. Categorization of the turbulence intensity into one of four ranges 0 - 1%, 2 - 5%, 6 - 11%, 12-16% and the integral scale size into one of three ~ 0.5D, ~ 1.0D, > 1.5D is sufficient. Essentially the intensity ranges cover, respectively, the basic types of flow regimes [24]: nearly laminar flows, the central core region of turbulent channel flows or the far outer region of wall turbulent shear flows, outside the central core region of channel flows and the near outer region of wall turbulent shear flows, and free turbulent shear flows such as occur downstream of cylinders, grids, and jets. The integral scale sizes are determined by the boundary layer thickness in wall flows and by the size of and distances from the sources in free shear flows.

The fluid force data utilized in this procedure was obtained in the central core region of turbulent channel flow or behind grids producing measured turbulence intensities and integral scales corresponding to available theory [36]. As such, they represent more homogeneous and isotropic flow conditions than the nonhomogeneous flows usually found in practice. Thus, if lower bounds on the turbulence intensity and upper bounds on the integral scale are estimated by testing or available data [24,36-38], then the design procedure should produce an upper bound on the actual response.

3. Response Estimation

A procedure to determine the mean square response in the direction normal to the mean velocity, the lift direction, is outlined after first checking to see that fluid-structure interaction does not occur. The same procedure can be applied to calculate response in the flow or drag direction, as illustrated in the examples.

a. Procedure applicability

Utilizing the largest velocity V_M and the lowest structural natural frequency f_o, for which motion transverse to the flow direction (the lift direction) is possible, determine if the reduced velocity satisfies

$$\frac{V_M}{f_o D} < 3.33 \ . \tag{28}$$

If not, then the procedure is not applicable because lift-direction lock-in is probable. If (28) is satisfied, determine if the reduced structural damping ratios c_1, calculated according to (2), satisfies

$$c_i > 1.2 \tag{29}$$

for each structural natural frequency with a reduced velocity less than 1. If (29) is not satisfied, then drag-direction fluid-structure interaction is probable and the procedure is not applicable.

b. Structural stiffness

If (29) is satisfied, then fluid-structure interaction is not probable and the mean square value of the lift direction forced response $\langle w^2 \rangle$ due to periodic and random vortex shedding can be estimated according to (20). Assuming that lift direction response occurs at the lowest frequency f_o, the reduced frequency $\bar{f}_o = f_o D/V_M$ can be calculated. With the c_o calculated in the previous subsection, the reduced stiffness K in (21) can be determined.

c. Reduced forces

The reduced force due to periodic vortex shedding $F_V = C_{LV}$ is determined by entering Fig. 2(b) or Table 2 at the Reynolds number

$$N_R = V_M D/\nu \tag{30}$$

and selecting the C_{LV} from the data with the closest, smaller turbulence intensity and closest, larger integral scale. Note that the data is relatively insensitive to integral scale length and that using the ideal flow data curve is always conservative.

The ideal flow data must be used to determine both C_{LR} and S at $N_R > 3 \times 10^5$ where the effects of turbulence are not yet known. Assuming that vortex shedding is strictly periodic for $N_R > 3 \times 10^5$ may or may not produce a more conservative response estimate than assuming random fluid forces. For a given force coefficient, which assumption produces the more conservative estimate depends upon the relative size of the multipliers γ_V and γ_R in (20). Most of the available information indicates that the forces will not be periodic until $N_R > 10^6$. Calculating responses due to both excitations and choosing the largest is recommended.

The reduced force due to turbulent buffeting $F_B = C_{LR}$ is determined from Fig. 3a. A value of $C_{LR} \cong 0.1$ appears appropriate for all turbulent flows. However for $N_R > 3 \times 10^5$, a $C_{LR} = 0$ should be employed for consistency when F_V is calculated assuming strictly periodic vortex shedding ($C_L = C_{LV}$), as discussed above. Utilizing the same logic for

determining response due to strictly random fluid forces at $N_R > 3 \times 10^5$, choose $C_{LV} = F_V = 0$. The random excitation estimate is expected to be closer in value to the actual response than the estimate based on strictly periodic vortex shedding, at least for $3 \times 10^5 < N_R < 10^6$.

The effective force for turbulent excitation of resonant response F_R is calculated according to (24) utilizing the spectral density of (16) where Φ_{LO} is selected from Table 2 for $N_R < 3 \times 10^5$. In interpolating Table 2, remember that a smaller turbulence intensity, a larger integral scale, or a larger Φ_{LO} will give a more conservative response prediction. For $N_R > 3 \times 10^5$, the response estimate associated with strictly periodic shedding is facilitated by choosing $\Phi_{LO} = F_R = 0$. The response estimate associated with assuming strictly random fluid forces, $F_V = 0$, for $N_R > 3 \times 10^5$ is facilitated by choosing $\Phi_{LO} = 0.042$, according to (19) with $C_L = C_{LR} = 0.1$.

d. Multipliers

The multipliers γ_V, γ_B, and γ_R can be calculated, according to (25-27), for each type of reduced force. Knowledge of the reduced frequency $\bar{f}_o$, the damping ζ_o, and the associated correlation length L_c is required. The least is known about the choice of L_c. For rigid, stationary cylinders the largest correlation lengths were measured for uniform, nonturbulent crossflow at $N_R < 3 \times 10^5$. The two-dimensionality, or axial independence, of the vortex shedding process is greatest for these ideal flow conditions. Still the correlation lengths are only three to six diameters. The measured effect of turbulence in the crossflow is always to reduce the correlation length. For $N_R > 3 \times 10^5$, all the correlation lengths measured have been one diameter or less. Both turbulence in the flow or flow exceeding the Reynolds number $N_R \sim 3 \times 10^5$, where the attached boundary layer first becomes turbulent in ideal crossflow, deteriorates the two-dimensionality of the vortex shedding process to various degrees.

In general, maintaining two-dimensionality of the vortex shedding process is very difficult for rigid, stationary cylinders. The surfaces of the cylinders must be very smooth with roughness height to diameter less than $\sim 10^3$, the flow turbulence intensity must be minimal or less than 0.5%, the $N_R < 10^5$, and the two-dimensionality of the mean flow velocity must be meticulously maintained. Flows along the axis of the cylinder, created by test section wall boundary layers, are so effective in destroying two-

dimensionality that most data has been taken utilizing two end plates which isolate a central section of the cylinder where measurements are made. The end plates, which are thin and short enough not to produce significant boundary flows of their own, are fixed on the cylinder, normal to its axis, and located outside the test section wall boundary layers.

Based on the above observations, a correlation length L_c of three diameters is recommended for calculating γ_V when $N_R < 3 \times 10^5$, and a correlation length of one diameter or the turbulence integral scale size, up to three diameters, is recommended for calculating γ_V when $N_R > 3 \times 10^5$ and γ_B and γ_R for all conditions. Conservative estimates of response are expected with these correlation lengths if the conditions which avoid fluid-structure interaction of subsection 3a. are satisfied: whereas maintaining a two-dimensional vortex shedding process is very difficult for a rigid stationary cylinder, if the fluid-structure lock-in phenomenon occurs the correlation lengths can approach the lengths of the vibrating cylinder.

4. Example Problem

a. Description

One of many thin-walled shroud tubes spaced six diameters apart is cantilevered into the plenum of a reactor system component where, channeled by baffle plates, it is exposed to crossflow along the part of its length between the baffle plates. The free end of the tube, which allows for thermal expansion, fits concentrically into a slightly larger, relatively short lower support sleeve attached to a relatively rigid support plate. See Fig. 6a for a typical tube.

The totally submerged, uniform tube is D_o = 100 mm in outside diameter, with a T = 10 mm wall thickness, and is 6 m in length. The tube inside diameter D_i = 80 mm. The shroud tube, made from 304 SS, contains and protects from the coolant flow a very flexible instrumentation control tube of the same material with a d_o = 25 mm outside diameter and t = 3 mm wall thickness. The control tube d_i = 19 mm. The remaining area inside the shroud and instrumentation tube is filled with fluid. The free end of the shroud tube fits into a sleeve which is larger in diameter by 2h = 1 mm and is three shroud tube diameters in length.

Sodium, at a temperature of 425°C, flows past the shrouds, and between the baffles, over a one meter length starting two meters from its fixed end. The normal operating flow rate through the channel formed by

the baffles divided by the open channel area, in a plane normal to the flow and containing the shroud, gives an average velocity of 0.3 to 3 m/sec depending on the tube location. The majority of the turbulence in the flow is expected to be created by the wakes of the upstream cylinders, when they exist, or by the turbulence in the channel where the array of shrouds begins.

No tests have been performed on this particular tube, but results from the testing of similar structures have shown that the cantilevered and higher mode damping in air may be less than 1% of critical damping when the amplitude of motion is small and the tube does not impact the baffle plates, where the shroud tube penetrates, or the lower support sleeve. When the response is large or initial misalignment is such that impacting occurs at the baffles, damping can increase to 4 or 5%. Testing of similar lower sleeve supports has shown that very little response or misalignment is required at the lower sleeve to change the lowest mode shape and frequency from that of a simple cantilevered beam to that of a fixed-simply supported beam.

The response is desired to determine shroud plate clearances which avoid baffle plate impacting and to make fatigue calculations.

b. Beam modeling

Because of the relative flexibility of the instrument line in the shroud, it is assumed to be mass carried by the shroud during fundamental mode vibration. With this assumption, the total mass per unit tube length can be calculated knowing that the mass density of 304 SS at 425°C is ρ_s = 7.85 x 10^3 kg/m^3 while that of sodium is ρ = 7.61 x 10^2 kg/m^3. Thus

$$m_s = \rho_s \pi[(D_o + D_i)T/2 + (d_o + d_i)t/2] = 23.81 \text{ kg/m}$$

$$m_c = \rho\pi[(D_i^2/4 - (d_o + d_i)t/2] = 3.67 \text{ kg/m} \qquad (31)$$

$$m_A = \rho\pi D_o^2/4 = 5.98 \text{ kg/m}$$

$$m_t = 33.45 \text{ kg/m}$$

for all lengths of the beam not in close proximity to other structures. Where the tube fits in the lower support sleeve, the added mass effect is

estimated [28] to be increased by the factor $(KD_o/2h) = (0.6)(100)/1 = 60$, where K is determined from Fig. 3 of [28]. With this factor

$$m_t' = 23.81 + 3.67 + 60(5.98) = 386.3 \text{ kg/m} . \tag{32}$$

Considering the tube to be cantilevered with a mass on its end, representing the added mass effect of the sleeve, the relative ratio of the beam mass to end mass is (6)(33.45)/(.3)(386.3) = 1.73. The cantilevered mode frequency and damping is estimated [28], see Appendix B, to be 1.02 Hz and 34% of critical damping, respectively. Considering the relatively large mass and damping effect of the fluid annulus alone, the beam can be expected to have a lowest mode response closer to a fixed-simply supported beam rather than a cantilevered beam. Also, the close fit of the tube in the support sleeve and fabrication tolerance buildup would justify modeling the lower sleeve as a simple support, at least. Because of the length of the sleeve, rotational support also could be rationalized, but using the lower fundamental frequency of the simple support model is more conservative.

For the fixed-simply supported beam model with $m_t = 33.45$ kg/m, $I = 2.90 \times 10^{-6}$ m^4, $E = 167 \times 10^9$ Pa (at 425°C), and L = 6 m, the lowest mode frequency of the beam can be calculated to be [39]

$$f_o = \frac{15.4}{2\pi L^2} \left(\frac{EI}{m_t}\right)^{1/2} = 8.2 \text{ Hz} . \tag{33}$$

The next two higher frequency modes occur at 26.5 and 55.2 Hz. The fundamental mode shape [39] is given approximately by

$$\psi_o(x) = \exp\left(-3.93 \frac{x}{L}\right) - \sqrt{2} \cos\left(3.93 \frac{x}{L} + \frac{\pi}{4}\right) \tag{34}$$

where

$$\int_o^L \psi_o^2(\xi) d\xi = L \tag{35}$$

and for L_e: $2m \leq x \leq 3m$

$$\int_{L_e} \psi_o^2(x) dx = 0.2742 \text{ L} . \tag{36}$$

The axial distance x is zero at the clamped end. The maximum value of

$\psi_o(x)$ is

$$\psi_o = 1.51 \qquad x = 0.58\ L \tag{37}$$

while $\psi_o = 0.96$ and 1.45 at the baffles where $x = 0.33\ L$ and $x = 0.5\ L$, respectively.

The reduced velocities associated with the beam fundamental frequency and specified range of flow velocities are

$$\frac{V}{f_o D_i} = \frac{0.3 \rightarrow 3}{(8.2)(0.1)} = 0.37 \rightarrow 3.7\ . \tag{38}$$

Thus the method will not be applicable for flow velocities greater than 2.7 m/sec, since (28) is not satisfied and lift direction lock-in is likely. For $V > 0.81$ m/sec, the reduced damping for the fundamental mode c_o must satisfy (29) to avoid drag direction lock-in and ensure applicability of the method. The higher beam modes do not have reduced velocities greater than one and therefore are not of concern.

To calculate c_o according to (2), the effective modal mass per unit length M_o must be determined. For a uniform beam $M_o > m_t$ according to (3). Assuming the beam is subject to a load along its entire length makes it easy to determine $M_o = m_t$ and $c_o = 55.23\ \zeta_o$ according to (2). Based on this c_o the design method would not be applicable, according to (2), for any $\zeta_o < 1.2/55.23 = 0.022$. Accounting for the fact that the beam is loaded over only part of its length, L_e: $2m < x < 3m$, the more exact value of $M_o = 3.65\ m_t$ is obtained from (3), utilizing (36). Based on the new $c_o = 201.4\ \zeta_o$, the design method would not be applicable for less than 0.6% of critical damping. Thus both conditions (28) and (29) are violated for part of the range of the component parameters: the largest flow velocities >2.7 m/sec and the smallest damping ratios <0.006.

Because the Reynolds numbers for $V > 2.7$ m/sec, $D = 0.1$ m, and $\nu = 3.16 \times 10^{-7}$ m^2/sec are large

$$N_R > 8.5 \times 10^5\ , \tag{39}$$

where lock-in response prediction methods are least reliable, a scale-model test would be indicated. Because of the expense of such testing, the recommendation to the designer would be to change the component design, if possible, so all conditions can be predicted with more confidence and, thus, lessen the need for scale model testing.

For purposes of calculating respose, the beam is taken to have a lowest frequency of f_o = 8.2 Hz, a fixed-simple mode shape given by (34), and a ζ_o = 0.01, c_o = 2.01, or a ζ_o = 0.04, c_o = 8.04.

c. Flow modeling

The mean flow velocity is taken to occur over the range of V = 0.3 m/sec to 2.7 m/sec with a corresponding Reynolds number range of $9.5 \times 10^4 \leq N_R \leq 8.5 \times 10^5$. The characterization of the flow turbulence cannot be as accurately defined and guidance from available literature [24,36-38] must be employed.

For the farthest upstream shroud tubes, the turbulence character will be governed by the upstream flow channel geometry. If it is long with respect to its width, then characterization as fully developed channel flow is appropriate. In the core region of the channel, the turbulence intensity is least, $\langle u^2 \rangle^{1/2}/V$ = 3 to 4%. Although the turbulence is nearly isotropic near the center of the core, in general it is anisotropic with the integral scale varying from 0.2 to 0.8 of the half channel width, or 0.1 m to 0.3 m, depending upon measurement direction [24]. If the channel is very short and forms a smooth intake from a much larger plenum region where the flow velocity is nearly zero, then the flow turbulence could be almost nonexistent. The extreme case, $\langle u^2 \rangle^{1/2}/V = 0$, will be considered in an example calculation.

In the array of tubes the scale of turbulence should be close to the size of the vortices shed, which is approximately the tube diameter in the short wake formation region allowed in the array. Depending on the array pattern, the tubes will be six to twelve diameters apart. For even larger distances downstream from a cylinder, the turbulence exhibits intensities greater than 20% and is still anisotropic [24]. The turbulence intensity 6-12 diameters downstream of a cylinder can be expected to be at least 15%. An example response calculation will be made for $\langle u^2 \rangle^{1/2}/V$ = 15% and $L_u = D$.

d. Lift direction response

Case 1 - Nonturbulent flow, lowest flow velocity, and smallest damping

Given: $\langle u^2 \rangle^{1/2}/V = 0$, V_M = 0.3 m/sec, $N_R = 9.5 \times 10^4$, $L_c = 3D$, D = 0.1 m, f_o = 8.2 Hz, and c_o = 2.01 for ζ_o = 0.01.

Results: $\bar{f}_o = 2.73$, $K^2 = 8.90 \times 10^7$, $F_V^2 = 0.25$, $\gamma_V = 0.184$ and

$$\langle w^2 \rangle^{1/2} = 2.27 \times 10^{-6} \psi_o(x) \quad \text{(meters)} \tag{40}$$

After calculating the reduced frequency from (12), the reduced stiffness K was calculated from (21). Entering Figs. 1-3 at $N_R = 9.5 \times 10^4$, $C_{LV} = C_L = 0.5$, $\bar{f}_V = S = 0.2$, and $C_{LR} = 0$ were chosen. Accordingly, the reduced force of periodic vortex shedding F_V could be calculated according to (22). The reduced forces of turbulent flow were assumed zero by definition: $F_B = F_R = 0$. Adopting the recommended correlation length $L_c = 3D$ for periodic vortex shedding, γ_V was calculated with (25). Because $\bar{f}_o \gg \bar{f}_V$ the structural part of the amplification was 1, the same as for static loads. Thus the multiplier γ_V actually is an attenuation ($\gamma_V < 1$) due to the relatively small correlation length, $L_c \ll L_e$.

Case 2 - Same as Case 1 but for largest damping

Given: As per Case 1 except $c_o = 8.04$ for $\zeta_o = 0.04$

Results: Same as for Case 1

Because $\bar{f}_V \ll \bar{f}_o$, the structural amplification is 1, static amplification, and the response predictions are not sensitive to structural damping variations.

Case 3 - Very turbulent flow, lowest flow velocity, and smallest damping

Given: $\langle u^2 \rangle^{1/2}/V = 15\%$, $L_u \approx D$, $L_c = D$, and see Case 1 for other parameters

Results: $\bar{f}_o = 2.73$, $K^2 = 8.90 \times 10^7$, $F_V^2 = 0.001$, $F_B^2 = 0.01$, $F_R^2 = 4.81 \times 10^{-6}$, $\gamma_V = 0.184$, $\gamma_B = 0.0613$, $\gamma_R = 4.82$, and

$$\langle w^2 \rangle^{1/2} = 3.0 \times 10^{-7} \psi_o(x) \quad \text{(meters)} \tag{41}$$

Case 1 $\bar{f}_o$, K, and N_R are applicable. Entering Figs. 1-3, $C_{LR} = 0.1$ and $C_{LV} = 0.03$ were chosen and allowed determination of F_V and F_B from (22-23). From (19), $\Phi_{LO} = 0.034$ for $C_{LR} = 0.1$ was calculated and employed to determine F_R by (24). The multiplier γ_V is the same as for Case 1. The γ_B is one-third as large, because the correlation length for turbulent excitation is assumed one-third that for periodic vortex shedding.

Whereas the periodic and buffeting force components produce nearly static responses, the random excitation produces response at f_o. The multiplier γ_R is a net amplification composed of a still larger structural amplification at $\bar{f}_o$ of 78.6 multiplied by a fluid correlation factor equal to γ_B. With these results, the displacement was calculated according to (20). A result worth noting is that the random response at the structural resonance is negligible in comparison to the buffeting response, while the vortex shedding response is about 15% at these low reduced velocities of high reduced frequencies.

Case 4 - Same as Case 3 except $\zeta_o = 0.04$, the largest damping

Since Case 3 response is nearly static and the random component of response is negligible for the smaller $\zeta_o = 0.01$, then the results will be the same as in Case 3 for the larger $\zeta_o = 0.04$.

Case 5 - Nonturbulent flow, highest flowrate, and largest or smallest damping

Given: Same as Case 1 or Case 2 except V = 27 m/sec and $N_R = 8.5 \times 10^5$

Results: $\bar{f}_o = 0.3$, $K^2 = 1.29 \times 10^4$, $F_V^2 = 0.01$, $\bar{f}_V = 0.23$, $\gamma_V = 1.07$, and

$$\langle w^2 \rangle^{1/2} = 9.22 \times 10^{-5} \psi_o(x) \quad \text{(meters)} \tag{42}$$

The above results were obtained following the same procedure as in Case 1 and Case 2: periodic vortex shedding was assumed to exist at this higher N_R. Notable quantitative difference with Case 1 was that the $C_{LV} = 0.1$ chosen from Fig. 2 is smaller. Also, because $\bar{f}_o$ is smaller by an order of magnitude, the excitation frequency $\bar{f}_V = 0.23$ is closer to the resonance frequency $\bar{f}_o = 0.3$, K^2 is smaller by almost four orders of magnitude, and γ_V is larger by almost an order of magnitude.

As suggested in the design procedure for his high Reynolds number range, the response assuming a random forcing function was calculated for comparison.

Results: $\bar{f}_o = 0.3$, $K^2 = 1.29 \times 10^4$, $F_B^2 = 0.01$, $F_R^2 = 3.64 \times 10^{-3}$, $\gamma_B = 0.0613$, $\gamma_R = 4.82$ for $\zeta_o = 0.01$ or $\gamma_R = 1.21$ for $\zeta_o = 0.4$, and

$$\langle w^2 \rangle^{1/2} = 1.072 \times 10^{-4} \psi_o(x) \text{ (meters)} \quad \text{for } \zeta_o = 0.01 \tag{43}$$

and

$$\langle w^2 \rangle^{1/2} = 5.69 \times 10^{-5} \psi_o(x) \text{ (meters)} \quad \text{for } \zeta_o = 0.04 \tag{44}$$

The calculation procedure followed was similar to that in Case 3 and Case 4. The only notable quantitative differences were that $C_{LV} = 0$ was chosen, $\bar{f}_o$ is an order of magnitude smaller, and most importantly the response is primarily (90%) due to random excitation resonance response rather than random buffeting. Thus the $\sim\sqrt{\zeta_o}$ dependence upon the amount of structural damping. Also note that for $\zeta_o = 0.01$, the response due to random excitation (43) is larger than that due to periodic vortex shedding (42).

Case 6 - Very turbulent flow, highest flow velocity, and largest and smallest damping

Fluid force data has not been taken at this high N_R for such turbulent flow. Based on extrapolating the existing information, no periodic vortex shedding would be expected and the best estimates of response would be the random force excitation results given directly above, (43) and (44).

e. Drag direction response

The same cases will be considered as for the lift direction.

Case 1 and Case 2 - Fluctuating drag response

Results: $\bar{f}_o = 2.73$, $K^2 = 8.90 \times 10^7$, $F_V^2 = 0.01$, $\bar{f}_V = 0.4$, $\gamma_V = 0.184$ and

$$\langle w^2 \rangle^{1/2} = 4.52 \times 10^{-7} \psi_o(x) \text{ (meters)} \tag{45}$$

For ideally nonturbulent, two-dimensional flow the fluctuating drag is periodic with a reduced frequency $\bar{f}_V$ or Strouhal number S twice that occurring in the lift direction and an amplitude, from Fig. 3, of $C_D' \approx 0.1$. Utilizing (22) with C_D' replacing C_{LV}, the F_V^2 was calculated. The K and γ_V are the same as for the lift direction analysis and RMS response is calculated according to (20) with $F_B = F_R = 0$. Note the response is smaller than in the lift direction (40), primarily due to a smaller force coefficient.

Case 1 and Case 2 - Steady drag response

Results: $\bar{f}_o = 2.73$, $K^2 = 8.9 \times 10^7$, $F_V^2 = 1.44$, $\gamma_V = 1.21$, $\bar{f}_V = 0$, and

$$w = 1.4 \times 10^{-5}\psi_o(x) \quad \text{(meters)} \tag{46}$$

An approximate value of the static deflection can be obtained from (20) by choosing $F_B = F_R = 0$, $F_V = C_D$, and $L_C = L_e = 2m$. From Fig. 4 a value of $C_D = 1.2$ was chosen and γ_V was calculated per (25). Of course, the deflection given above is not an RMS value as reported for the fluctuating response. The static deflection is approximate to the degree the fundamental dynamic mode shape represents the static deflection curve. For uniform beams the two are usually quite close. Note the static deflection (46) is larger than the dynamic response (45), primarily due to the larger static force coefficients.

Case 3 - Fluctuating drag response

Results: $\bar{f}_o = 2.73$, $K^2 = 8.9 \times 10^7$, $F_B^2 = 0.01$, $F_R^2 = 9.25 \times 10^{-3}$,

$\gamma_B = 0.0613$, $\gamma_R = 4.82$, and

$$\langle w^2 \rangle^{1/2} = 2.25 \times 10^{-6}\psi_o(x) \quad \text{(meters)} \; . \tag{47}$$

The $\bar{f}_o$ and K are the same as for Cases 1 and 2 above, but F_V is assumed zero while $F_B = C_D' = 0.1$ was chosen from Fig. 4. Corresponding to a $C_D' = 0.1$, a $\Phi_{DO} = 0.044$ was determined from (15), and F_R^2 was determined with (24) and (13). Using the same γ_B and γ_R as employed in the lift direction, the RMS response was determined with (20). Note this response is larger than the lift direction response (41) which was due primarily to turbulent buffeting. In contrast, for the drag direction, resonant response to random excitation predominates over buffeting response. It is larger than the resonant response in the lift direction, because of the larger bandwidth of Φ_D as compared to Φ_L. See (13), (16), and Fig. 5. Essentially, for the same force coefficient, more energy exists at higher frequencies where the structural natural frequencies are restricted, by design, to occur. Thus, as will be seen in the results of Case 4, a $\sqrt{\zeta_o}$ dependence on damping exists.

Case 3 - Steady drag response

Results: Same as for Case 1 and Case 2 except $F_V^2 = 0.16$ and

$$w = 4.67 \times 10^{-6}\psi_o(x) \quad \text{(meters)} . \tag{48}$$

The static deflection varies in direct proportion to $F_V = C_D$. For 15% turbulence intensity $C_D = 0.4$ instead of 1.2, see Fig. 4, and the static deflection is proportionally smaller.

Case 4 - Fluctuating drag response

Results: Same as for Case 3 except $\gamma_R = 1.21$ and

$$\langle w^2 \rangle^{1/2} = 1.15 \times 10^{-6}\psi_o(x) \quad \text{(meters)} . \tag{49}$$

As discussed above, the RMS response is primarily due to random excitation at resonance and therefore exhibits a $\sqrt{\zeta_o}$ dependence on damping. Since Case 3 has one-fourth the damping of this case, it will have twice the response. Of course, the static response does not depend upon ζ_o and therefore is the same.

Case 5 and Case 6 - Fluctuating drag response

Results: $\bar{f}_o = 0.3$, $K^2 = 1.29 \times 10^4$, $F_B^2 = 0.01$, $F_R^2 = 6.59 \times 10^{-2}$, $\gamma_B = 0.0613$, $\gamma_R = 4.82$ for $\zeta_o = 0.01$, $\gamma_R = 1.21$ for $\zeta_o = 0.04$ and

$$\langle w^2 \rangle^{1/2} = 4.97 \times 10^{-4}\psi_o(x) \text{ (meters)} \quad \text{for } \zeta_o = 0.01 \tag{50}$$

and

$$\langle w^2 \rangle^{1/2} = 2.5 \times 10^{-4}\psi_o(x) \text{ (meters)} \quad \text{for } \zeta_o = 0.04 \tag{51}$$

Since no periodic vortex shedding has been observed for this high $N_R = 8.5 \times 10^5$, $F_V = 0$ was assumed, and a force coefficient of $C_D' = F_B = 0.1$ was chosen from Fig. 3. Corresponding to $C_D' = 0.1$, F_R^2 was determined as in cases 3 and 4 directly above. Again the dependence on $\sqrt{\zeta_o}$ is present. Note the drag direction response amplitudes (50) and (51) are several times larger than those of the lift direction (42-44).

Case 5 and Case 6 - Steady drag response

Results: $\bar{f}_o = 0.3$, $K^2 = 1.29 \times 10^4$, $\bar{f}_V = 0$, $F_V^2 = 0.25$, $\gamma_V = 1.21$, and

$$w = 4.84 \times 10^{-4} \psi_o(x) \quad \text{(meters)} . \tag{52}$$

The same procedures were followed as for Case 1. The quantitative differences are the smaller value of K and $F_V = C_D = 0.5$, obtained from Fig. 4 for $N_R = 8.5 \times 10^5$.

f. Discussion

The responses calculated according to the design procedure are very small and on the order of the static drag deflection for the example considered, but the example is typical of structures which satisfy the constraints, (28) and (29), of the design method: only significantly off-resonant response which is sufficiently damped is allowed. The condition requiring off-resonant response is primarily responsible for the small motions, and it is worth discussing what may happen if (28) is violated for the example considered.

First the assumption will be made that lock-in occurs. Several methods for determination of nonlinear lock-in response are available, but an order of magnitude estimate can be calculated utilizing the linear response relation (20) and some physically observed estimates of the system parameters which occur during lock-in. In the lift direction, for example,

Given: $V = 2.7$ m/sec, $L_c = 2$m, $\bar{f}_o = \bar{f}_V = 0.25$, $\zeta_o = 0.01$, $C_L = C_V = 1.0$

then

Results: $K^2 = 2.55 \times 10^3$, $F_V^2 = 1.0$, $F_B = F_R = 0$, $\gamma_V = 3025$, and

$$\langle w^2 \rangle 1/2 = 0.071 \psi_o(x) \quad \text{(meters)} . \tag{53}$$

Even though the flow and structural parameters are the same as for the smallest damping situation discussed in Case 5, almost one diameter of motion is predicted. This is why the lock-in phenomenon is avoided or only allowed to occur for large values of reduced damping c_o.

To make the predictions, lock-in and the coincidence of the frequency of structural motion and vortex shedding at $\bar{f}_o = \bar{f}_V = 0.25$ were presumed. This is a somewhat contrived condition, for lock-in won't occur

for the actual large separation in values of $\bar{f}_V = 0.23$ and $\bar{f}_o = 0.3$. However, the frequency at which lock-in occurs is relatively unimportant. In going from an $\bar{f}_o = 0.3$ to $\bar{f}_o = 0.23$ the response is increased only by a factor of 1.7. Whereas the fact that $\bar{f}_V = \bar{f}_o$ was assumed, increases γ_V from 1.07 to 3025, which translates into an increase of response by a factor of 55. The increase in γ_V is due to two factors. First, assuming total correlation of the vortex shedding during lock-in, results in an increase in L_c from 0.3 m to 2 m, a factor of 6.67. Second, the major increase, a factor of 453, is due to the large structural amplification which occurs when periodic excitation occurs at the structural response frequency. Also, the lock-in was presumed to amplify the lift coefficient from 0.1 to 1.0, a factor of 10, which translates into an additional increase in response by a factor of 10.

As noted in the discussion of Case 6 for lift direction motion, force data is not known for very turbulent flows at high N_R. In addition the literature is contradictory on the effect of large flow turbulence on the lock-in phenomenon at low or high N_R. If large turbulence does not allow the lock-in phenomenon to occur, the data of Figs. 1-3 are applicable and even at resonance, when $\bar{f}_V = \bar{f}_o$, the response will be small. In fact, it would only be a couple of times larger than the lift response calculated for random excitation in Case 6, (43) and (44).

CONCLUDING REMARKS

The procedure developed herein for prediction of dynamic structural response of a circular cylinder in turbulent crossflow has shown that very small amplitudes of motion can be expected for typical reactor components, unless lock-in occurs. The use of the procedure is prohibited for those conditions where lock-in has been observed in relatively nonturbulent flow. Whether the lock-in phenomenon will occur for the prohibited conditions in very turbulent flow has not been established.

The possibility exists that for very turbulent flow lock-in does not occur and the small amplitudes predicted by this procedure are valid. The existence of another set of operating conditions for which the usually very destructive lock-in phenomenon can be avoided would be useful to reactor component designers. This emphasizes the importance of conducting a fundamental investigation to determine whether or not the lock-in phenomenon occurs for very turbulent flows.

ACKNOWLEDGMENTS

This work was performed under the sponsorship of the Office of Reactor Research and Technology, U. S. Department of Energy.

The comments of M. W. Wambsganss were appreciated.

REFERENCES

1. Blevins, R. D., Flow-Induced Vibration, Van Nostrand, 1977.

2. Turula, P., and Mulcahy, T. M., "Computer Modeling of Flow-Induced In-Reactor Vibrations," J. Power Division, Proc. ASCE 103(1), 37-49 (1977).

3. Mulcahy, T. M., and Miskevics, A. J., "Fluid Forces on Circular Cylinders in Turbulent Crossflow," (In preparation).

4. Roshko, A., "Experiments on the Flow Past a Circular Cylinder at Very High Reynolds Number," J. Fluid Mech. 78, 561-576 (1961).

5. Ericson, L. E., and Redding, J. P., "Criterion for Vortex Periodicity in Cylinder Wakes," AIAA 17(9), 1012-1013 (1979).

6. Sarpkaya, T., "Vortex-Induced Oscillations - A Selective Review," Trans. ASME, J. Appl. Mech. 46, 241-258 (1979).

7. Loiseau, H., and Szechenyi, E., "Analyse Expérimentale Des Portances sur un Cylindre Immobile soumis a un Ecoulement Perpendiculaire a son Axe a des Nombres de Reynolds Elevevés," La Recherche Aerospatial, No. 5, 279-291 (1972).

8. Graham, C., "A Survey of Correlation Length Measurements of the Vortex Shedding Process behind a Circular Cylinder," Engineering Projects Laboratory Report 76028-1, Massachusetts Institute of Technology (1966). Available from U. S. Dept. of Commerce Clearinghouse AD 650 849.

9. Szechenyi, E., "Supercritical Reynolds Number Simulation for Two-Dimensional Flow over Circular Cylinders," J. Fluid Mech. 70(3), 529-542 (1975).

10. Jones, G. W., "Unsteady Lift Forces Generated by Vortex Shedding about a Large, Stationary, and Oscillating Cylinder, ASME Paper 68-FE-36 (1968).

11. Schmidt, L. V., "Fluctuating Force Measurements upon a Circular Cylinder at Reynolds Numbers up to 5×10^6," Meeting on Ground Wind Load Problems in Relation to Launch Vehicles, NASA Langley Research Center, June 7-8, 1966, NASA TM 57779, pp. 19.1-19.17 (1966).

12. Fung, Y. C., "Fluctuating Lift and Drag acting on a Cylinder in a Flow at Supercritical Reynolds Numbers," J. Aerospace Sciences 27(11), 801-814 (1960).

13. Keefe, R. T., "An Investigation of the Fluctuating Forces acting on a Stationary Circular Cylinder in a Subsonic Stream and of the Associated Sound Field," University of Toronto Institute for Aerospace Studies Report 76 (1961).

14. Connors, H. J., "Vortex Shedding Excitation and the Vibration of Circular Cylinders," Flow-Induced Vibration Design Guidelines, Ed. P. Y. Chen, ASME publication PVP-52, 47-74 (June 1981).

15. Güven, O., Farell, C., and Patel, V. C., "Surface-Roughness Effects on the Mean Flow Past Circular Cylinders," J. Fluid Mech. 98(4), 673-701 (1980).

16. King, R., "On Vortex Excitation of Model Piles in Water," J. Sound Vib. 29(2), 169-188 (1973).

17. Erickson, L. E., "Karman Vortex Shedding and the Effect of Body Motion," AIAA 18(8), 935-944 (1980).

18. Naudascher, E., and Rockwell, D., Practical Experiences with Flow-Induced Vibrations, Springer-Verlag, New York (1980).

19. Sarpkaya, T., and Isaacson, M., Mechanics of Wave Forces on Offshore Structures, Van Nostrand Reinhold, New York, Chapter 8 (1981).

20. Martin, W. W., Currie, I. G., and Naudascher, E., "Streamwise Oscillations of Cylinders," J. Eng. Mech., ASCE 107(EM3), 589-607 (1981).

21. Skop, R. A., and Griffin, O. M., "On a Theory for the Vortex-Excited Oscillations of Flexible Cylindrical Structures," J. Sound Vib. 41(3), 263-274 (1975).

22. Mulcahy, T. M., "Flow-Induced Vibration Testing Scale Modeling Relations," Flow-Induced Vibration Design Guidelines, ASME publication PVP-52, Ed. P. Y. Chen, 111-126 (June 1981).

23. Chen, S. S., "Fluid Damping for Circular Cylindrical Structures," Nucl. Eng. Des. 63(1), 81-100 (1981).

24. Hinze, J. O., Turbulence, McGraw Hill, New York (1975).

25. Farell, Cesar, "Flow Around fixed Circular Cylinders: Fluctuating Loads," J. Eng. Mech. Div., ASCE 107(EM3), 565-588 (1981).

26. So, R. M. C., and Savkar, S. D., "Buffeting Forces on Rigid Circular Cylinders in Crossflows," J. Fluid Mech. 105, 297-425 (1981).

27. Bruun, H. H., and Davies, P. O. A. L., "An Experimental Investigation of the Unsteady Pressure Forces on a Circular Cylinder in a Turbulent Cross Flow," J. Sound Vib. 40(4), 535-559 (1975).

28. Mulcahy, T. M., "Fluid Forces on Rods Vibrating in Finite Length Annular Regions," J. Appl. Mech. 102(2), 234-240 (1980).

29. Meirovitch, L., Analytical Methods in Vibrations, The MacMillan Company, London (1967).

30. Davenport, A. G., and Novak, M., "Vibration of Structures Induced by Wind," Shock and Vibration Handbook, Ed. C. M. Harris and C. E. Crede, pp. 29-21 to 29-43 (1976).

31. Mulcahy, T. M., and Wambsganss, M. W., "Flow-Induced Vibration of Nuclear Reactor System Components," The Shock and Vibration Digest 8(7), 33-45 (1976).

32. Wambsganss, M. W., and Mulcahy, T. M., "Flow-Induced Vibration of Nuclear Reactor Fuel," The Shock and Vibration Digest 11(11), 11-22 (1979).

33. Mulcahy, T. M., "A Fluid Damping Distortion in FIV Scale Modeling," Nucl. Eng. and Des. 63(1), 101-107 (1981).

34. Dong, R. G., "Size Effect in Damping Caused by Water Submersion," J. Structural Division, Proc. ASCE 105(ST5), 847-857 (1979).

35. Stevenson, J. D., "Structural Damping Values as a Function of Dynamic Response Stress and Deformation Levels," Nucl. Eng. Des. 60, 211-237 (1980).

36. Naudascher, E., and Farell, C., "Unified Analysis of Grid Turbulence," J. Eng. Mech. Div., ASCE 96(EM2), 121-141 (1970).

37. Corrsin, S., "Turbulence: Experimental Methods," Fluid Dynamics II, Encyclopedia of Physics (VIII/2), Ed. S. Flügge, pp. 525-590 (1963).

38. Laws, E. M., and Livesey, J. L., "Flow Through Screens," Annual Review of Fluid Mechanics 10, 247-266 (1978).

39. Blevins, R. D., "Formulas for Natural Frequency and Mode Shape," Van Nostrand Reinhold, New York (1979).

40. Savkar, S. D., and So, R. M. C., "On the Buffetting Response of a cylinder in Turbulent Cross Flow," General Electric Report, GEAP-24149 (Sept. 1978). Available from NTIS.

Table 1. Grid turbulence characteristics and coefficients associated with force spectral density functional form (13) [3]

Grid	Intensity (%)	Scale (mm)	Φ_{DO}	C'_{DC}
OP	3	50	0.100	0.15
HC	2	50	0.100	0.15
2(493)	4	13	0.032	0.09
24(191)	10	10	0.010	0.05
24(107)	16	10	0.014	0.06
52(493)	11	25	0.027	0.08
52(338)	15	24	0.026	0.08

Table 2. Fluid force coefficients [3]

Grid	$N_R x 10^{-5}$	C_L	Φ_{LO}	C_{LR}	C_{LV}	C_{DU}	C_D	S	ΔS
OP	0.24	0.48	0.069	0.14	0.33	1.29	1.20	0.18	0.01
	0.45	0.47	0.069	0.14	0.33	1.13	1.06	0.19	0.01
	0.71	0.46	0.069	0.14	0.31	1.31	1.21	0.19	0.01
	0.94	0.34	0.069	0.14	0.19	1.16	1.08	0.18	0.00
	1.38	0.25	0.20	0.24	0.01	1.00	0.94	0.18	0.03
	1.89	0.19	0.12	0.18	0.01	0.67	0.64	0.20	0.10
HC	0.22	0.42	0.033	0.10	0.32	1.00	0.94	0.20	0.02
	0.45	0.45	0.041	0.11	0.34	1.37	1.27	0.19	0.01
	0.68	0.38	0.041	0.11	0.27	1.36	1.26	0.20	0.01
	0.90	0.23	0.033	0.10	0.13	1.27	1.18	0.20	0.00
	1.37	0.19	0.021	0.08	0.11	1.25	1.17	0.19	0.01
	1.86	0.24	0.19	0.24	0.00	1.03	0.97	0.19	0.05
2	0.22	0.59	0.074	0.15	0.44	1.50	1.38	0.19	0.01
	0.43	0.43	0.074	0.15	0.28	1.13	1.06	0.20	0.01
	0.71	0.25	0.074	0.15	0.10	0.82	0.78	0.20	0.02
	0.90	0.19	0.074	0.15	0.04	0.64	0.61	0.22	0.02
	1.2	0.10	0.038	0.11	-0.01	0.44	0.42	0.18	0.05
	1.6	0.07	0.021	0.08	0.00	0.35	0.34	0.17	0.04
24(191)	0.29	0.21	0.036	0.10	0.11	0.70	0.67	0.19	0.01
	0.58	0.10	0.024	0.08	0.02	0.39	0.38	0.23	0.01
	0.86	0.08	0.020	0.07	0.01	0.35	0.34	0.20	0.07
	1.15	0.08	0.023	0.08	0.01	0.33	0.32	0.18	0.07
	1.69	0.10	0.025	0.09	0.01	0.35	0.34	0.18	0.07
	3.52	0.11	0.028	0.09	0.02	0.38	0.37	0.18	0.07
24(107)	0.32	0.14	0.052	0.12	0.02	0.43	0.41	0.20	0.05
	0.64	0.11	0.037	0.10	0.01	0.34	0.33	0.20	0.06
	0.97	0.12	0.037	0.10	0.02	0.37	0.36	0.20	0.23
	1.28	0.12	0.037	0.10	0.02	0.38	0.37	0.18	0.22
	1.63	0.13	0.052	0.12	0.03	0.45	0.43	0.19	0.23
	1.85	0.15	0.052	0.12	0.03	0.44	0.42	0.19	0.23
	2.58	0.15	0.052	0.12	0.01	0.44	0.42	0.19	0.11
52(493)	0.20	0.43	0.087	0.16	0.27	0.99	0.93	0.20	0.00
	0.40	0.25	0.060	0.13	0.11	0.50	0.48	0.21	0.01
	0.63	0.17	0.037	0.10	0.06	0.48	0.46	0.23	0.06
	0.78	0.13	0.037	0.10	0.03	0.44	0.42	0.22	0.07
	1.18	0.14	0.037	0.10	0.03	0.40	0.39	0.19	0.07
	1.60	0.14	0.037	0.10	0.04	0.41	0.40	0.19	0.08
52(338)	0.22	0.37	0.10	0.17	0.20	0.61	0.58	0.21	0.01
	0.47	0.19	0.06	0.13	0.06	0.63	0.60	0.21	0.04
	0.61	0.17	0.06	0.13	0.04	0.48	0.46	0.21	0.07
	0.91	0.17	0.06	0.13	0.04	0.47	0.45	0.20	0.08
	1.04	0.16	0.06	0.13	0.03	0.38	0.37	0.20	0.08
	1.36	0.16	0.06	0.13	0.03	0.35	0.34	0.19	0.08

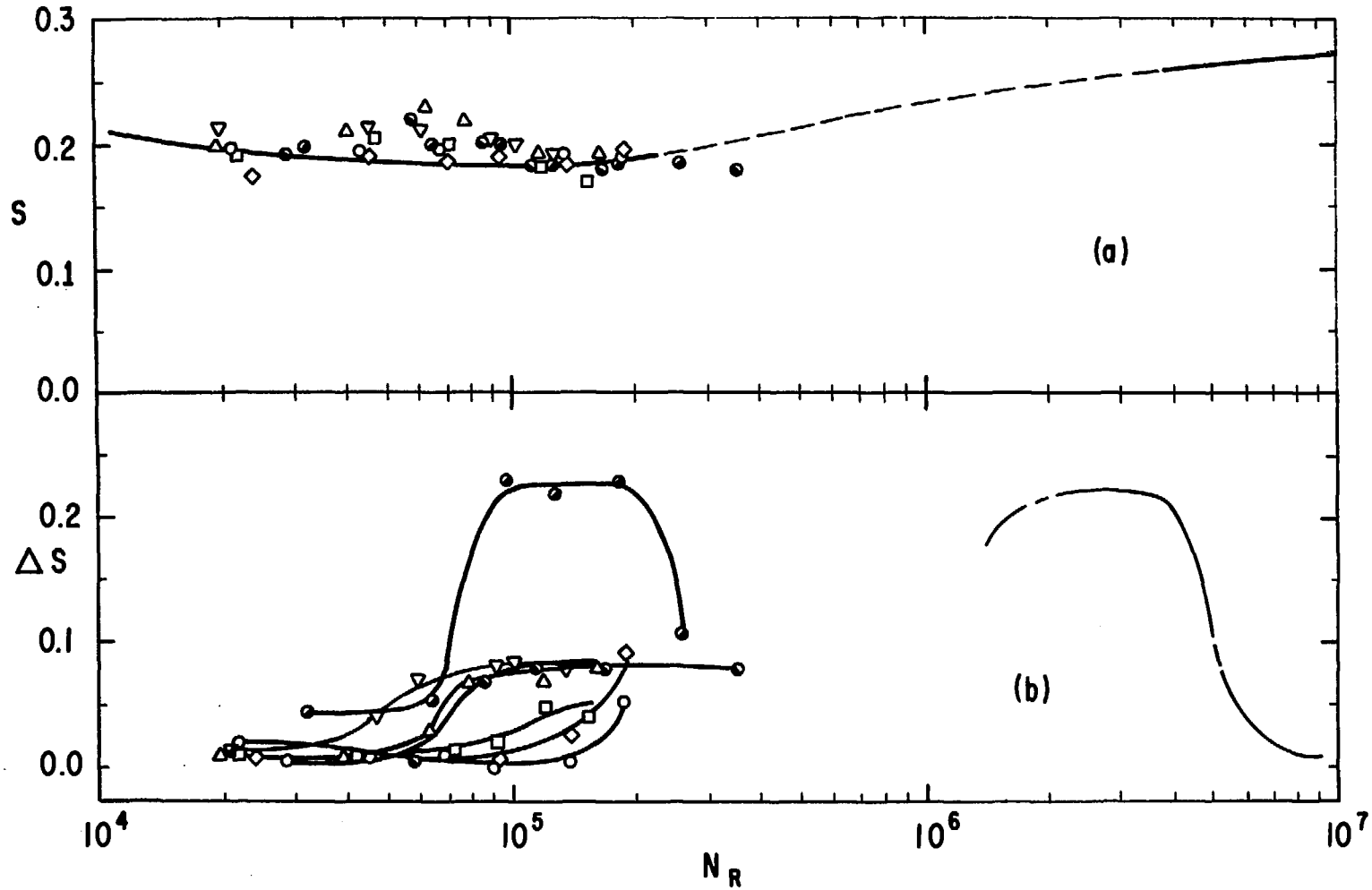

Fig. 1. (a) Strouhal number S. (b) Half-power bandwidth ΔS. Turbulent flow (grid in Table 1, symbol): OP,◇; HC, ○; 2, □; 24 (191), ◔; 24 (107), ◪; 52 (493), Δ; 52 (334), ▽. Ideal crossflow S ————, with - - - - representing trend for sporadic data [5]. Ideal crossflow ΔS — - — [10].

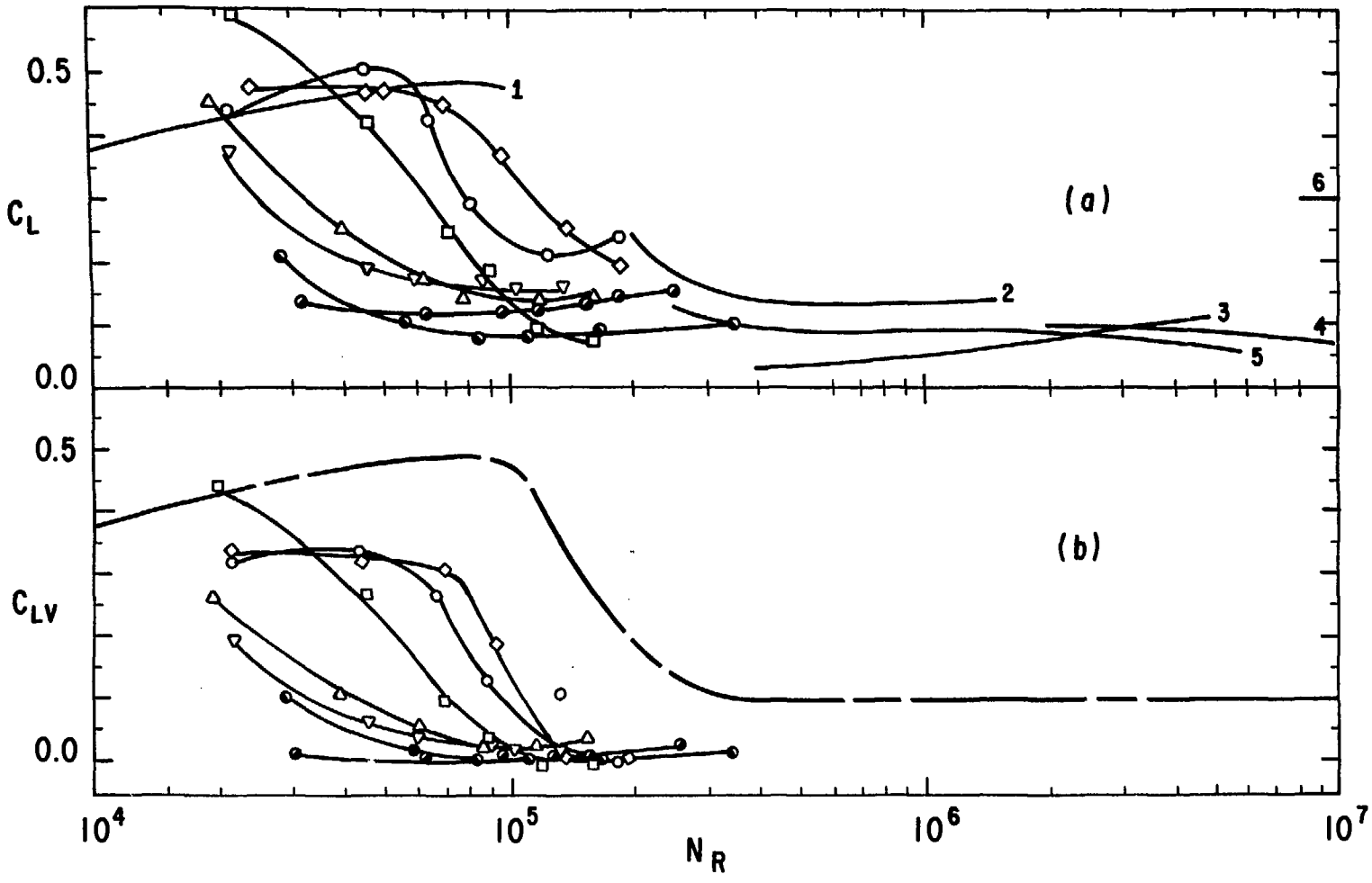

Fig. 2. (a) Total lift force coefficients C_L. (b) Narrow band lift coefficients C_{LV}. Ideal crossflow curves: 1 [13], 2 [12], 3 [11], 4 [10], 5 [7], and 6 [9]. Upper bound curve —— - —— for ideal crossflow data. See Fig. 1 for turbulent flow data notation.

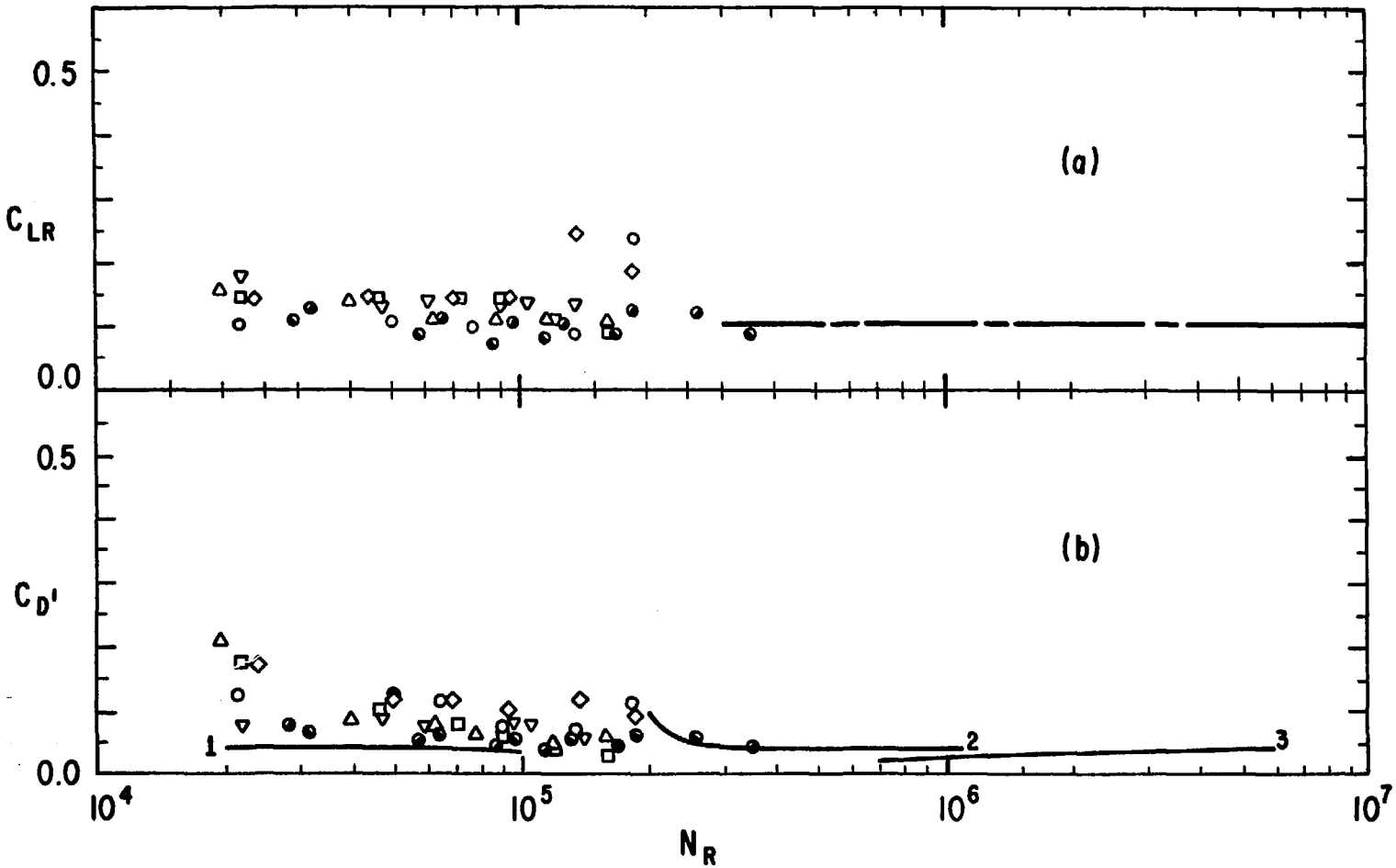

Fig. 3. (a) Wide band lift coefficient C_{LR}. (b) Fluctuating drag coefficient C_D'. See Figs. 1 and 2 for notation.

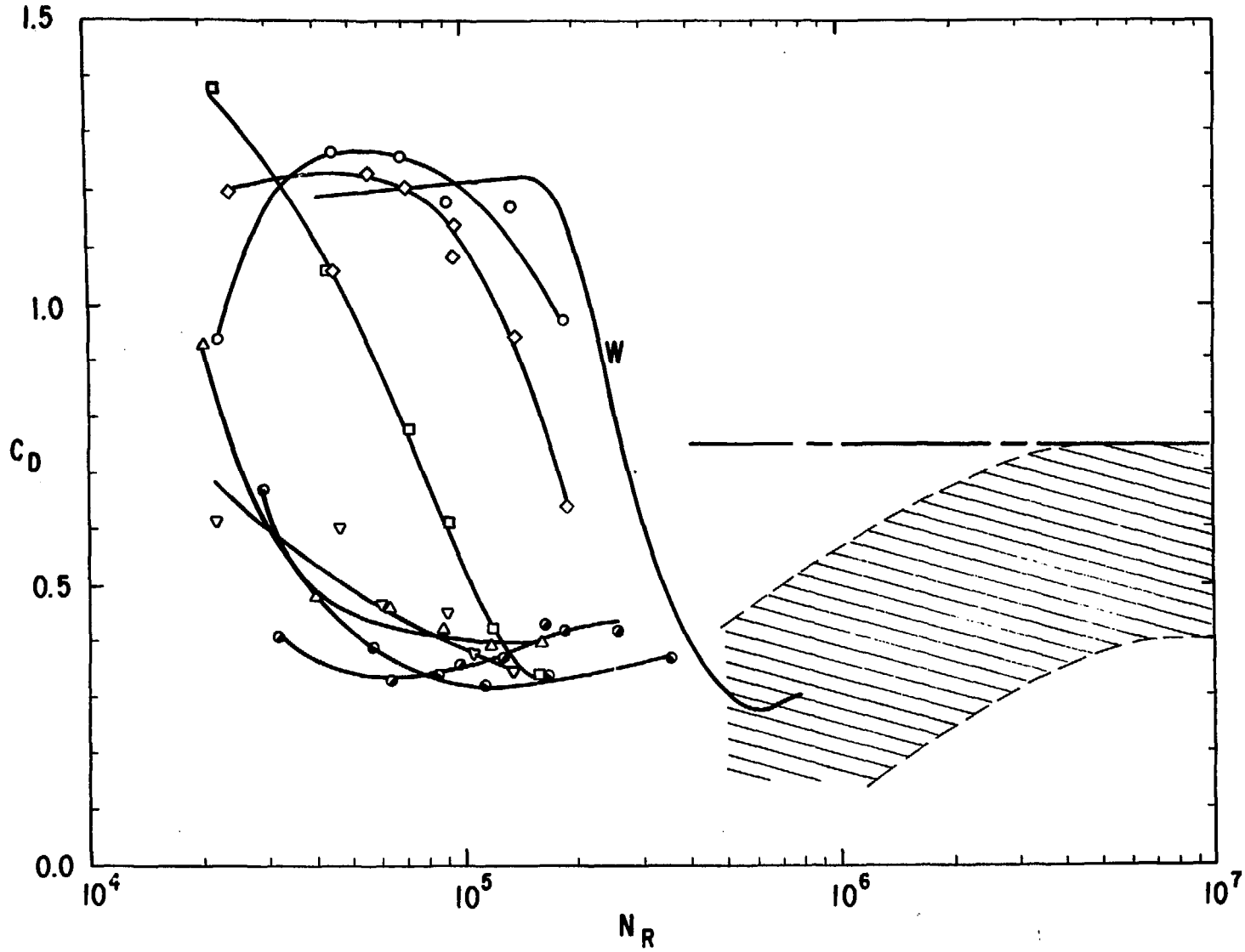

Fig. 4. Mean drag coefficient C_D. Ideal crossflow data notation: Wieselberger from [4] ——— W, scatter band (////) of existing data, and bounding curve — - —. See Fig. 1 for turbulent flow data notation.

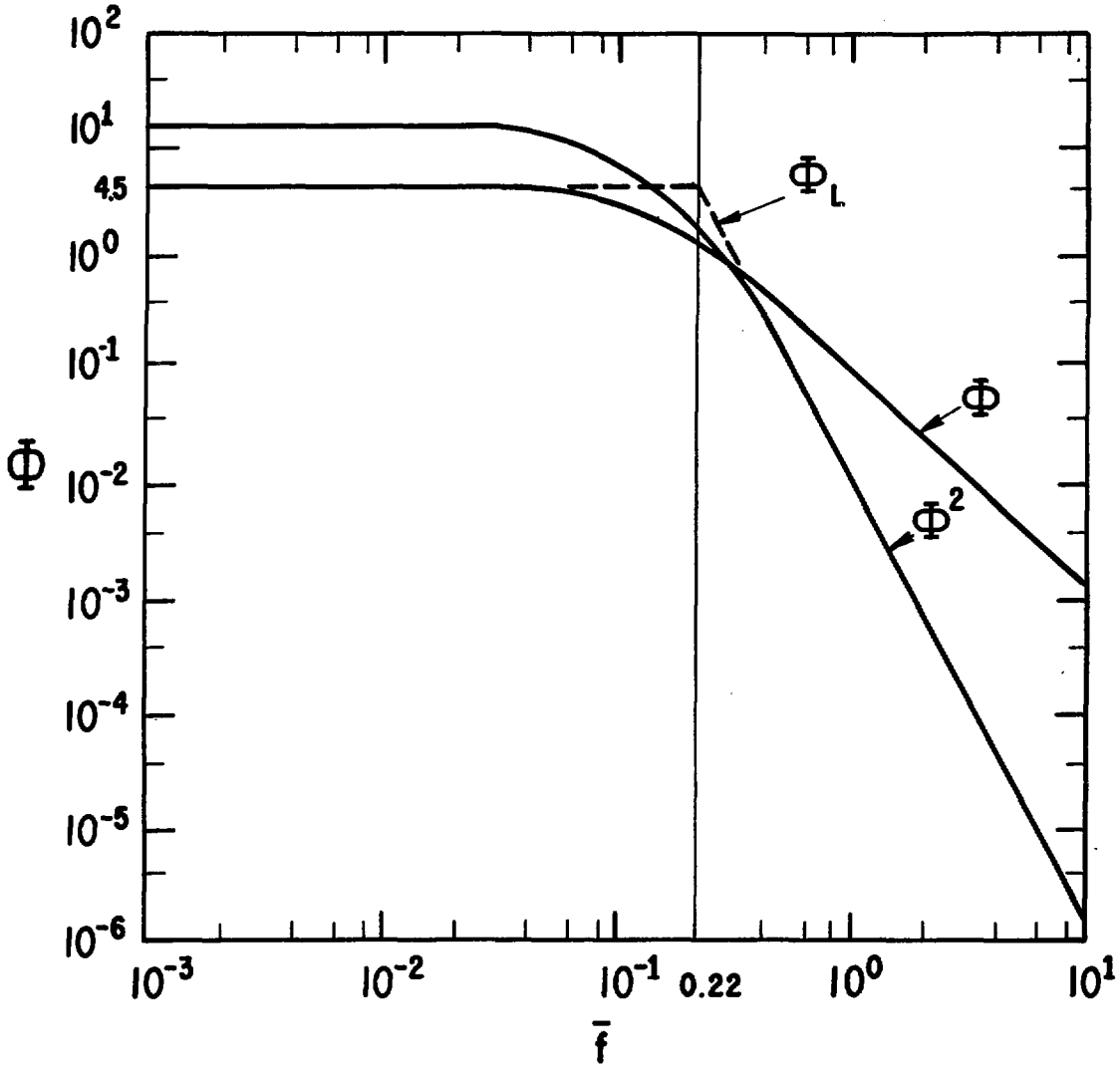

Fig. 5. Turbulence velocity fluctuation spectral density functional form $\Phi(\bar{f})$ shown with $\Phi^2(\bar{f})$ and a linear bound Φ_L to Φ, $\bar{f} < 0.22$, and Φ^2, $\bar{f} > 0.22$.

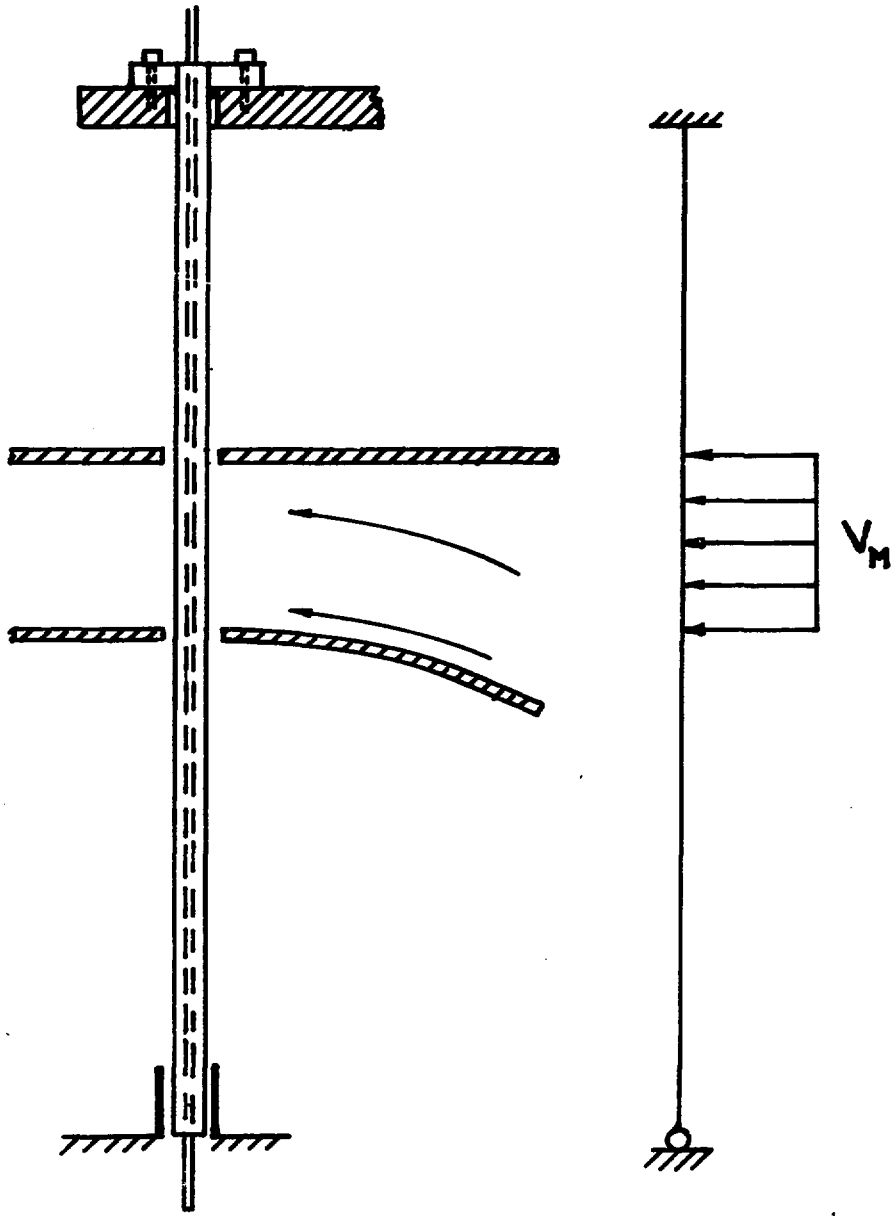

Fig. 6. Example problem (a) component and (b) beam model.

APPENDIX A - DYNAMIC RESPONSE ANALYSIS

1. Free Vibrations

The modal analysis of beams is classical and is included here for completeness and consistency of notation and treatment.

a. Equation of motion [29]

The governing equation of motion for the free vibrations of a beam is

$$m(x)\frac{\partial^2 w}{dt^2} + L(w) = 0 \tag{1-1}$$

where L( ) is a stiffness operator per unit length.

b. Solution

Assuming that separation of variables is possible, the solution

$$w(x,t) = \sum_{i=1}^{\infty} \psi_i(x) r_i(t) \tag{1-2}$$

is substituted into (1-1) to give

$$\sum_{i=1}^{\infty} \left[m(x)\psi_i(x)\frac{d^2 r_i}{dt^2} + r_i L(\psi_i) \right] = 0$$

which requires for a stable oscillatory (noncritical damped) system

$$\frac{1}{r_i}\frac{d^2 r_i}{dt^2} = -\omega_i^2 \; ; \qquad \frac{L(\psi_i)}{m(x)\psi_i} = \omega_i^2 \tag{1-3}$$

where the eigenvalue ω_i, in rad/sec, is often given in cycles/sec: $f_i = \omega_i/2\pi$. The solution to the first of the above equations is the real part of

$$r_i = R_i e^{\hat{i}\omega_i t} \tag{1-4}$$

and ψ_i is the solution of the eigenvector equation

$$L(\psi_i) = \omega_i^2 m(x)\psi_i(x) \; . \tag{1-5}$$

The above equations are solved, with the appropriate boundary conditions, for the frequencies ω_i and the mode shape function eigenvectors ψ_i.

c. Eigenvector properties

Assuming that the system is self-adjoint (see Appendix B)

$$\int_0^L [\psi_i L(\psi_j) - \psi_j L(\psi_i)]dx = 0 \tag{1-6}$$

then the eigenvectors are orthogonal, in the sense

$$\int_0^L m(x)\psi_i(x)\psi_j(x) = 0 \qquad i \neq j \tag{1-7}$$

for distinct frequencies $\omega_j \neq \omega_i$. This can be shown by combining (1-5) and (1-6) to give

$$(\omega_i^2 - \omega_j^2) \int_0^L m(x)\psi_i \psi_j dx = 0 \tag{1-8}$$

2. Forced Vibrations

The equation of motion of a beam subject to a time varying load p(t) is given by [29]

$$m(x) \frac{\partial^2 w}{\partial t^2} + \frac{\partial}{\partial t} C(w) + L(w) = p \tag{2-1}$$

assuming that the beam is subject to a damping operator C(w). The solution to (2-1) can be expressed easily in terms of the free vibration eigenvectors $\psi_i(x)$ if C(w) takes the form of generalized viscous damping per unit length

$$C(w) = C_1 L(w) + C_2 m(x) w \tag{2-2}$$

where C_1 and C_2 are constants. Because damping is difficult to define, the assumption (2-2) usually is made and has proven to be a satisfactory procedure where beam natural frequencies are adequately separated.

a. Modal decomposition

Assuming that the system possesses orthogonal self-adjoint eigenvectors, then the solution to (2-1) can be expanded in the series

$$w(x,t) = \sum_{i=1}^{\infty} \psi_i(x) q_i(t) \tag{2-3}$$

where q_i is the modal displacement. Substituting (2-3) into the equation of motion, multiplying by $\psi_j(x)$, and integrating the result over the beam length gives

$$\sum_{i=1}^{\infty} \left[\frac{d^2 q_i}{dt^2} \int_o^L m\psi_j\psi_i d\xi + \frac{dq_i}{dt} \int_o^L \psi_j C(\psi_i) d\xi \right.$$
$$\left. + q_i \int_o^L \psi_j L(\psi_i) dx = \int_o^L p\psi_j dx \right] . \qquad (2\text{-}4)$$

From the orthogonality condition (1-7), the eigenvector equation (1-5), and the form of damping (2-2), the single equation uncouples into

$$\ddot{q}_i + 2\omega_i\zeta_i q_i + \omega_i^2 q_i = p_i/m_i \qquad i = 1, 2, \ldots, \infty \qquad (2\text{-}5)$$

where the ( ) has been employed to denote time derivatives and

$$\int_o^L \psi_j C(\psi_i) dx = 2\omega_i\zeta_i \int_o^L m(x)\psi_i\psi_j dx \; \delta_{ij} \qquad (2\text{-}6)$$

with $2\omega_i\zeta_i = C_1\omega_i^2 + C_2$. The modal fraction of critical damping is ζ_i, and the modal mass per unit length is

$$m_i = \int_o^L m(\xi)\psi_i^2(\xi) d\xi \; / \int_o^L \psi_i^2(\xi) d\xi \quad . \qquad (2\text{-}7)$$

The modal force per unit length is

$$p_i(t) = \int_o^L p(\xi,t)\psi_i(\xi) d\xi \; / \int_o^L \psi_i^2(\xi) d\xi \quad . \qquad (2\text{-}8)$$

For the special case of static deformation: $q_i = \ddot{q}_i = 0$ and (2-9)

$$q_i = p_i/k_i$$

where (2-10)

$$k_i = m_i\omega_i^2$$

is the modal stiffness.

b. Fourier analysis

For nondeterministic fluid forces p(x,t), statistical analysis of the response is appropriate and is often done in the frequency domain. The spectral density of the response can be determined by Fourier transform

analysis of the modal equation of motion (2-5). Taking the Fourier transform of both sides of (2-5) gives

$$-\omega^2 Q_i + 2\omega\omega_i\zeta_i Q_i\hat{i} + \omega^2_i Q_i = P_i/m_i \tag{2-11}$$

where

$$P_i(\omega) = \int_0^L P(\xi,\omega)\psi_i(\xi)d\xi \;/\; \int_0^L \psi_i^2(\xi)d\xi \tag{2-12}$$

and the Fourier transforms are given by

$$Q_i(\omega) = \int_{-\infty}^{+\infty} q_i(t)e^{-\hat{i}\omega t}dt \tag{2-13}$$

and

$$P(x,\omega) = \int_{-\infty}^{+\infty} p(x,t)e^{-\hat{i}\omega t}\,dt \quad . \tag{2-14}$$

Solving for $Q_i(\omega)$,

$$Q_i(\omega) = P_i(\omega)/k_i z_i(\omega) \tag{2-15}$$

where

$$z_i(\omega) = 1 - (\omega/\omega_i)^2 + \hat{i}2\zeta_i(\omega/\omega_i) \tag{2-16}$$

is the complex structural mode amplification factor.

A similar Fourier transform formulation can be made in terms of frequency f in cycles per second rather than ω in radians per second. The results are of the same form as derived above and can be obtained by replacement in (2-11) to (2-16) of $P(\omega)$, $P_i(\omega)$, $Z_i(\omega)$, with $P(f)$, $P_i(f)$, $Z_i(f)$ and substitution of

$$\omega = 2\pi f \tag{2-17}$$

and

$$\omega_i = 2\pi f_i \tag{2-18}$$

where they occur explicitly. Future reference to dependences on ω or f will be deleted except where explicitly required. Note several different definitions of Fourier transforms and their inverse are employed in the literature, and care must be exercised when comparing data and results.

Having determined the Fourier transform of Q_i, the transform of the displacement can be determined

$$W = \sum_{i=1}^{\infty} \psi_i P_i / k_i z_i . \tag{2-19}$$

By substituting (2-19) and (2-12) into the correlation theorem [29]

$$\lim_{T\to\infty} \frac{1}{T} \int_{-T/2}^{T/2} w(x,t)w(x',t+\tau)d\tau = \lim_{T\to\infty} \frac{1}{T} \int_{-\infty}^{+\infty} W^*(x,f)W(x',f)e^{\hat{i}2\pi f\tau}df . \tag{2-20}$$

Then letting $x = x'$ and $\tau = 0$, the mean square displacement

$$\langle w^2 \rangle = \sum_{i=1}^{\infty} \sum_{j=1}^{\infty} (\psi_i \psi_j / k_i k_j) \int_{-\infty}^{\infty} S_{ij} / z_i z_j df \tag{2-21}$$

is obtained recognizing

$$S_{ij}(f) = \lim_{T\to\infty} \frac{1}{T} P_i^*(f) P_j(f) \tag{2-22}$$

is the cross spectral density ($-\infty < f < \infty$) of the modal forces per unit length.

3. Special Cases

The results of the previous section can be simplified for many situations which occur in practical applications.

a. Single mode response

Assuming that the majority of the response occurs in the lowest mode

$$\langle w^2 \rangle = (\psi_o^2 / k_o^2) \int_{-\infty}^{+\infty} S_{oo} / |z_o|^2 df \tag{3-1}$$

where the first mode amplification factor is

$$|z_o|^2 = [1 - (f/f_o)^2]^2 + [2\zeta_o f/f_o]^2 \tag{3-2}$$

and the first mode generalized force spectral density is

$$S_{oo}(f) = \left[\int_o^L \psi_o^2 d\xi\right]^{-2} \int_o^L \int_o^L S_p(\xi,\xi',f)\psi_o(\xi)\psi_o(\xi')d\xi d\xi' \tag{3-3}$$

where $S_p(x,x',f)$ is the cross spectral density of $p(x,t)$

$$S_p(x,x',f) = \lim_{T\to\infty} \frac{1}{T} P^*(x,t)P(x',t) \ . \tag{3-4}$$

b. $\ell_c \ll L$

If the correlation length for $p(x,t)$, Δ, is small in comparison to the beam length L, then (3-3) further simplifies to

$$S_{oo}(f) = \left[\int_o^L \psi_o^2 d\xi\right]^{-2} \int_o^L S_p(\xi,f)\ell_c(\xi,f)\psi_o^2(\xi)d\xi \tag{3-5}$$

where only knowledge of the single point spectral density $S_p(x,f)$ of $p(x,t)$ is required and an estimate of the correlation length

$$\ell_c(x,f) = \int_{-\Delta/2}^{\Delta/2} r(x,x+\ell,f)d\ell \qquad \Delta \ll L \tag{3-6}$$

which formally is defined in terms of the coherence function (Appendix D)

$$r(x,x',f) = \frac{S_p(x,x',f)}{[S_p(x,f)S_p(x',f)]^{1/2}} \ . \tag{3-7}$$

However, ℓ_c can be conservatively estimated based on existing data.

c. Single-sided spectra

In the measurement of spectral densities, most often the single-sided estimates $\phi_p(x,f)$, $0 \leq f \leq \infty$, are determined rather than the double-sided $S_p(x,f)$, $-\infty \leq f \leq \infty$. No generality is lost employing $\phi_p = 2S_p$, $0 \leq f \leq \infty$, because S_p is symmetric in f. In the same fashion, a single-sided generalized force spectral density ϕ_{ij} can be employed instead of S_{ij}. Both ϕ_{oo} and ϕ_p are employed in the main text.

d. Constant velocity and correlation length

If the velocity and correlation length are constant, $V = V_M$ and $\ell_c = L_c$, respectively, over the length of the beam L_e where fluid excitation occurs, then the generalized force spectral density (3-5) can be simplified to

$$\Phi_{oo}(f) = L_c\left[\int_{L_e} \psi_o^2 d\xi \ / \ \left(\int_o^L \psi_o^2 d\xi\right)^2\right] \Phi_p \tag{3-8}$$

where the normalized spectrum Φ_{oo} is employed which has been obtained by multiplication of ϕ_{oo} by the factor $V_M/D(1/2\ \rho\ V_M^2 D)^{-2}$, as in section 4 of the text, (14) and (17). Substitution of (3-8) into (3-1) yields, with some algebraic manipulation, the normalized mean square displacement

$$\frac{\langle w^2 \rangle}{\psi_c^2 D^2} = \gamma\ F^2/K^2 \tag{3-9}$$

where

$$\gamma F^2 = \left(L_c \Big/ \int_{L_e} \psi_o^2 d\xi\right) \int_o^\infty \Phi_p \Big/ |z_o|^2 d\bar{f}\ . \tag{3-10}$$

$$K = 4\pi \bar{f}_o^2\ c_o (2\zeta_o)^{-1} \tag{3-11}$$

The γ will be interpreted as a multiplier of a reduced force F and K as a reduced stiffness. Also, the reduced stiffness can be interpreted as the product of the reduced damping or mass c_o, see (2) of the text, times the reduced frequency squared or acceleration $4\pi^2 \bar{f}_o^2 = \bar{\omega}_o^2$. Note in (3-12) that $|z_o|^2$ depends parametrically upon the damping factor ζ_o and the fundamental frequency $\bar{f}_o$. See (3-2).

Once the structure's free vibrational response has been characterized, in terms of $\bar{f}_o$, ψ_o, ζ_o, and c_o, the dynamic mean square response can be determined from (3-9) after specification of L_c and determination of γF^2 for the particular fluid force operative.

e. Idealized Φ_p

The integration for γF^2 in (3-10) is obtained readily for several extreme combinations of normalized fluid force spectral densities Φ_p and structural properties, as characterized by $|z_o|$. When the fluid force per unit length excitation occurs in a very narrow frequency band centered about the reduced frequency $\bar{f}_v$, then

$$F = F_V = C_{LV} \tag{3-12}$$

$$\gamma = \gamma_V = \frac{L_c \Big/ \int_{L_e} \psi_o^2 d\xi}{\left[1 - (\bar{f}_v/\bar{f}_o)^2\right]^2 + \left[2\zeta_o f_v/f_o\right]^2} \tag{3-13}$$

where C_{LV} is the (RMS) lift coefficient for the narrow band excitation.

The largeat value for γ_V occurs when the excitation and fundamental frequency coincide

$$\gamma_V = \frac{L_c}{(2\zeta_o)^2 \int_{L_e} \psi_o^2 d\xi} . \tag{3-14}$$

In this case, the multiplier is a measure of structural amplification and attenuation due to lack of fluid force correlation.

In the case of wide band excitation where the energy of excitation is limited to occur in a frequency band well below the fundamental frequency, called buffeting, the response is nearly static in character and is given by

$$F = F_B = C_{LR} \tag{3-15}$$

$$\gamma_B = L_c \Big/ \int_{L_e} \psi_o^2 d\xi \tag{3-16}$$

as can be seen from (3-13) letting $f_v/f_o \approx 0$ and C_{LR} represent the RMS lift coefficient for wide band random excitation. In this case, the multiplier is a measure of fluid force correlation attenuation since static structural amplification is one.

When the fluid force excitation occurs in a wide frequency band which is nearly constant in magnitude $\Phi_p(\bar{f}_o)$ and includes the fundamental reduced frequency $\bar{f}_o$, then the integral of (3-10) can be evaluated explicitly [29] to give

$$F_R = \bar{f}_o \Phi_p(\bar{f}_o) \tag{3-17}$$

$$\gamma_R = \frac{\pi}{4} \zeta_o^{-1} L_c \Big/ \int_{L_e} \psi_o^2 d\xi . \tag{3-18}$$

f. General Φ_p

When the excitation force occurs over a wide frequency band which has a maximum near $\bar{f}_o$, then (3-10) cannot be evaluated explicitly. However, for Φ_p whose variation with $\bar{f}$ is gradual, the γF^2 can be approximated by adding the separate results (3-15) to (3-18) [30]. Thus, in the general case, where the excitation force consists of a component

distributed over a wide band of frequencies superimposed on a periodic component, an estimate of the mean square response is given by

$$\frac{\langle w^2 \rangle}{\psi_o^2 D^2} \approx \frac{1}{K^2} \left[\gamma_V F_V^2 + \gamma_B F_B^2 + \gamma_R F_R^2 \right] \qquad (3\text{-}19)$$

which is an upper bound.

APPENDIX B - EXAMPLE DETAILS

For the shroud tube in the close fitting sleeve of the example problem, assume the damping operator of Appendix A (2-1) is entirely viscous in nature

$$C(w) = C(x)w(x) \ , \tag{1}$$

where C is the damping coefficient. This is an accurate representation [29] for small motion which is all that can occur without impacting. The fundamental mode damping ratio is

$$\zeta_o = \frac{1}{2\omega_o} \int_o^L C\psi_o^2 dx \ / \ \int_o^L m\psi_o^2 dx \ , \tag{2}$$

assuming the normal modes are uncoupled. If

$$m(x),C(x) = \begin{matrix} m,0 & 0 \leq x \leq L \\ m',C & L \leq x \leq L + \Delta L \end{matrix} \tag{3}$$

and $\Delta L \ll L$, then

$$\zeta_o = \frac{C}{2\omega_o m'} \left[1 + \frac{mL}{m'\Delta L} \frac{1}{\psi_1^2(L)L} \int_o^L \psi_1^2 dx\right]^{-1} \ . \tag{4}$$

For a cantilevered mode $\psi_1^2(L) > \psi_1^2(x)$, thus

$$\zeta_o > \frac{C}{2\omega_o m'} \left[1 + mL/m'\Delta L\right]^{-1} \tag{5}$$

where C depends upon frequency. For the example problem, the frequency of the fundamental mode is [39]

$$f_o = \frac{1}{2\pi} \left[\frac{3EI}{L^3(m'\Delta L + 0.24\ mL)}\right]^{1/2} \ . \tag{6}$$

Since $mL = 6(33.45)$ kg/m, $m'\Delta L = 0.3(386.3)$, $E = 167 \times 10^9$ Pa for 304 SST at 425°C, and

$$I = \frac{1}{64} \pi((.1)^4 - (.08)^4) = 2.90 \times 10^{-6} m^4 \tag{7}$$

then $f_o = 1.02$ Hz. Knowing the frequency, and the kinematic viscosity $\nu = 3.16 \times 10^{-7}$ m^2/sec, an approximation for the damping coefficient is available [28]. The viscous penetration depth divided by the gap size is

$$\left(\frac{\delta_V}{h}\right) = \left[\frac{2\nu}{h^2(2\pi f_o)}\right]^{1/2} = 0.634 \ . \tag{8}$$

Then from Figs. 2 and 3 of [28]

$$C = (0.6)(2)(100)m'_A\omega_o$$

which gives finally

$$\zeta_o > 0.6 \frac{m'_A}{m'} [1 + mL/m'\Delta L]^{-1/2} = 0.337$$

or 34% of critical damping, which is quite large.